

Monte Carlo Simulations of Metal-Poor Star Clusters^{★,★★}

Martina Fagiolini^{1,2}, Gabriella Raimondo³, and Scilla Degl’Innocenti^{1,2}

¹ Dipartimento di Fisica, Università di Pisa, Largo B. Pontecorvo 3, I-56126 Pisa, Italy

² INFN, Sezione di Pisa, Largo B. Pontecorvo 3, I-56126 Pisa, Italy

³ INAF, Osservatorio Astronomico di Teramo, Via M. Maggini, I-64100, Teramo, Italy

Received date / Accepted date

ABSTRACT

Context. Metal-poor globular clusters (GCs) can provide a probe of the earliest epoch of star formation in the Universe, being the oldest stellar systems observable. In addition, young and intermediate-age low-metallicity GCs are present in external galaxies. Nevertheless, inferring their evolutionary status by using integrated properties may suffer from large *intrinsic* uncertainty caused by the discrete nature of stars in stellar systems, especially in the case of faint objects.

Aims. In this paper, we evaluate the *intrinsic* uncertainty (due to statistical effects) affecting the integrated colours and mass-to-light ratios as a function of the cluster integrated visual magnitude (M_V^{tot}), which represents a quantity directly measured. We investigate the case of metal-poor single-burst stellar populations with age from a few million years to a likely upper value for the Galactic globular cluster ages (~ 15 Gyr).

Methods. Our approach is based on Monte Carlo techniques for randomly generating stars distributed according to the cluster’s mass function.

Results. Integrated colours and mass-to-light ratios in different photometric bands are checked to be in good agreement with the observational values of low-metallicity Galactic clusters; the effect of different assumptions on the Horizontal Branch (HB) morphology is shown to be not relevant, at least for the photometric bands explored here. We present integrated colours and mass-to-light ratios as a function of age for different assumptions on the cluster total V magnitude. We find that the *intrinsic* uncertainty cannot be neglected. In particular, in models with $M_V^{tot} = -4$ the broad-band colours show an *intrinsic* uncertainty so high as to prevent precise age evaluation of the cluster. The effects of different assumptions on the initial mass function and on the minimum mass for which carbon burning is ignited on both integrated colours and mass-to-light ratios are also analyzed. Finally, the present predictions are compared with recent results available in the literature, showing in some cases non-negligible differences.

Key words. stars: evolution – (Galaxy:) globular clusters: general – galaxies: star clusters

1. Introduction

A key issue in astronomy is to determine ages and chemical compositions of those stars and stellar systems that are needed to reconstruct the formation and evolution of galaxies. Toward this goal, the analysis of the stellar clusters population in external galaxies and in the Milky Way is fundamental for tracing the history of the par-

ent galaxy (see, e.g. Cote et al. 1998; West et al. 2004). Contrarily to the situation in the Galaxy, in which massive ($\approx 10^5 \div 10^6$ stars) stellar clusters are old ($\gtrsim 10$ Gyr) and metal poor ($[Fe/H] \lesssim -0.7$), observations indicate that in the Magellanic Clouds, in the Local Group galaxies, and even in galaxies beyond the Local Group, massive stellar clusters spread a large range of both metallicity and age; thus they are considered the main indicators of stellar formation events in the galaxies history (Larsen 2000; Matteucci et al. 2002; Harris 2003). Hereinafter we will use the term “globular clusters” (GCs) to signify massive clusters of whatever age and chemical composition.

GCs have the advantage to be bright objects, and then to be easily observed beyond the Local Group. In addition, they are thought to be simple stellar pop-

Send offprint requests to: Gabriella Raimondo, e-mail: raimondo@oa-teramo.inaf.it

[★] All the tables (i.e. for models with $M_V^{tot} = -4, -6, -8$) are available in electronic form at the CDS via anonymous ftp to [cdsarc.u-strasbg.fr](ftp://cdsarc.u-strasbg.fr) (130.79.128.5) or via <http://cdsweb.u-strasbg.fr/cgi-bin/qcat?J/A+A/>

^{★★} All the figures are available as colored figures in the electronic edition of the Journal.

ulations (SSPs), consisting of a gravitationally bound group of stars born at nearly the same moment, and with a nearly identical chemical composition. The integrated broad-band colours, line indices, and mass-to-light ratios, we observe from those systems, are the unique observational tools to understand their properties. Since the pioneering work by Tinsley (1972), different groups have developed population synthesis models, e.g. (Brocato et al. 1990b; Charlot & Bruzual 1991; Buzzoni 1993; Bressan et al. 1994; Worthey 1994; Maraston 1998; Kurth et al. 1999; Brocato et al. 2000; Vazdekis 1999; Girardi et al. 2000; Anders & Fritze-v. Alvensleben 2003; Bruzual & Charlot 2003; Maraston 2005, and references therein) in order to interpret such observables.

Besides the *systematic* uncertainties due to different sets of stellar evolutionary tracks and different spectral libraries—used to transform the models from luminosity and effective temperature to observable quantities—(see e.g. Charlot et al. 1996; Maraston 1998; Brocato et al. 2000; Bruzual & Charlot 2003; Yi 2003), broad-band colours may suffer from large *intrinsic* fluctuations caused by the discrete nature of the number of stars in the system. The first studies were carried out in the optical by Barbaro & Bertelli (1977) - for population I clusters - and Chiosi et al. (1988)- for intermediate ($Z=0.001$) and solar metallicity -, while Santos & Frogel (1997) analyzed the case for near infrared (NIR) bands. Among other results, the quoted authors concluded that it is necessary to include stochastic effects when deriving ages and metallicities from integrated broad-band colours.

Most studies normalized their theoretical predictions to the total number of stars or total mass in the cluster, while Brocato et al. (1999, 2000) derived the mean broad-band colours and the corresponding dispersions as a function of the cluster visual magnitude (M_V^{tot}) for selected values of ages. This approach directly links theory and observations and it is crucial when the cluster age and metallicity are inferred from the observed broad-band colours, especially for clusters at the faint end of the GC luminosity function.

In this paper we extend the investigations by Brocato et al. (1999) and Brocato et al. (2000) and we analyze stochastic effects not only on broad-band colours, but also on mass-to-light ratios as a function of the adopted cluster visual magnitude, M_V^{tot} . We provide a comprehensive study on this problem by investigating the time-evolution of both integrated colours and mass-to-light ratios for a fine grid of stellar ages and for three different values for M_V^{tot} . The analysis is carried out using new single-burst low-metallicity models ($Z=0.0002$) based on the updated stellar models database by Cariulo et al. (2004). We choose this metallicity because the metal-poor GCs can provide a probe of the earliest epoch of star formation in the Universe, being the oldest stellar systems observable. In addition, young and intermediate age low metallicity GCs are present in external galaxies (Larsen & Richtler 1999, 2000). For these reasons, and also because an analysis of young metal-poor clusters gives an idea on

how old GCs appeared when they formed, we explore a wide range of ages ($7.7 \leq \log[age(yr)] \leq 10.3$). We note that we did not take into account redshift effects thus our calculations can be used only for objects with a redshift lower than about 0.1.

The results are compared with a sample of low-metallicity clusters in the Galaxy with different HB morphology, chosen as prototypes of the old stellar populations studied in this work. The present theoretical predictions are also compared with recent results available in the literature showing in some cases non-negligible differences.

We also discuss the influence of the adopted Initial Mass Function (IMF) on integrated colours and mass-to-light ratios and the effect of changing the maximum mass (M_{up}) for which carbon burning is not ignited, due to effects of the degenerate pressure and neutrino energy losses in the core. The assumption of a fixed M_V^{tot} can lead to a peculiar behaviour when varying the shape of the IMF, since an adjustment of the total number of stars might be required to keep the M_V^{tot} value fixed.

The layout of the paper is the following. In Section 2 the ingredients of the stellar population synthesis code are outlined, together with a brief description of the method adopted to derive the integrated quantities. In Section 3 we show the comparison of the theoretical results with selected observations of galactic globular clusters. Then, we discuss the uncertainties affecting integrated colours (Section 4) and mass-to-light ratios (Section 5), together with a comparison with previous works.

2. Description of the code

Synthetic CMDs and magnitudes presented in this paper are based on the stellar population synthesis code developed by Brocato et al. (1999, 2000), and Raimondo et al. (2005)¹. In this section, we briefly describe the main ingredients and recall the method used to derive integrated magnitudes and colours, referring to the cited papers for more details.

2.1. Ingredients

The present SSP models rely on the evolutionary tracks of the “Pisa Evolutionary library”² for masses $M \geq 0.6M_\odot$ (Cariulo et al. 2004). The input physics adopted in the models has already been discussed in Cariulo et al. (2004). We only point out here that the models take into account atomic diffusion, including the effects of gravitational settling, and thermal diffusion with diffusion coefficients given by Thoul et al. (1994); radiative acceleration (see e.g. Richer et al. 1998; Richard et al. 2002) is not included. The effects of rotation (see e.g. Maeder & Zahn 1998; Palacios et al. 2003) are also not included.

¹ <http://www.oa-teramo.inaf.it/SPoT>

² <http://astro.df.unipi.it/SAA/PEL/Z0.html>. Data files are also available at the CDS.

Convective regions, identified following the Schwarzschild criterion, are treated with the mixing length formalism. We use throughout the canonical assumption of inefficient overshooting, so the He burning structures are calculated according to the prescriptions of canonical semiconvection induced by the penetration of convective elements in the radiative region (Castellani et al. 1985). The efficiency and presence of a mild overshooting are still open questions (Barmina et al. 2002; Brocato et al. 2003); however, as discussed in Yi (2003), a modest amount of overshooting (i.e. $H_P \sim 0.2$, see also Brocato et al. 2003) influences only integrated colours with ages $\lesssim 1.5$ Gyr for a maximum amount of ≈ 0.1 mag. The models span the evolutionary phases from the main sequence up to C ignition or the onset of thermal pulses (TP) in the advanced Asymptotic Giant Branch (AGB) in the mass range $0.6 \div 11 M_\odot$. This allows us to calculate stellar population models in the age range $\approx 50 \text{ Myr} \div 20 \text{ Gyr}$.

Beyond the early-AGB phase, thermally pulsating (TP) stars have been simulated in the synthesis code using the analytic formulas of Wagenhuber & Groenewegen (1998) which describes time evolution of the core mass, and luminosity of TP stars. These formulae include three important effects: (i) the fact that the first pulses do not reach the full amplitude, (ii) the hot bottom burning process that occurs in massive stars, and (iii) the third dredge-up. The effective temperature (T_e) of each TP-AGB star has been evaluated using prescriptions by Renzini & Voli (1981), considering the appropriate slope $d \log(L/L_\odot)/d \log(T_e)$ of the adopted evolutionary tracks. The analytic procedure ends up providing the time evolution of the temperature and luminosity for a given mass (see for details Raimondo et al. 2005).

Mass loss affecting Red Giant Branch (RGB) stars and early-AGB stars has been taken into account following prescriptions by Reimers (1975):

$$\dot{M}_R = -4 \cdot 10^{-13} \eta_R \cdot LR/M, \quad (1)$$

while during the TP phase we adopted the Baud & Habing (1983) mass-loss rate:

$$\dot{M}_{BH} = \mu LR/M_e. \quad (2)$$

Here, L, R, M, M_e are, respectively, the star luminosity, radius, total mass, and envelope mass in solar units; $\mu = -4 \cdot 10^{-13} (M_{e,0}/M)$, being $M_{e,0}$ the envelope mass at the first TP. Eq. 2 is a modification of the Reimers formula with $\eta_R = 1$ which also includes a dependence on the actual mass envelope. The initial-final mass relation is applied by Dominguez et al. (1999), and no white dwarfs (WD) more massive than $1.1 M_\odot$ are accepted (Prada Moroni & Straniero 2005).

In this paper the TP phase is included but we do not adopt any separation between C-rich and O-rich TP-stars. All stars are oxygen-rich when they enter the AGB phase. Whether or not they become C-stars depends primarily on the efficiency of the third dredge-up (TDU) occurring

on the TP-AGB phase, and the extent and time-variation of the mass-loss (e.g. Marigo et al. 1999; Straniero et al. 2003). In low-metallicity stars ($Z < 0.004$), the amount of oxygen in the envelope is so low that a few thermal pulses are sufficient to convert an O-rich star into a C-star (Renzini & Voli 1981). In addition, the smaller the metallicity the smaller the minimum mass for the onset of TDU (e.g. Straniero et al. 2003). On the other hand, TP-AGB stars may experience episode of strong mass loss, that in the case of low mass stars may cause a reduction of the envelope mass that may delay or even prevent the TDU occurrence and the formation of C-rich stars (Marigo et al. 1999). In conclusion, the presence of C-rich stars may affect NIR-bands luminosity and its uncertainty in the case of low-metallicity, intermediate-age massive clusters (see e.g. Maraston 1998), while at the typical age of Galactic globular clusters their presence become more uncertain, as confirmed by the fact that AGB stars in GGC are all observed to be oxygen-rich, so that carbon does not appear to have been dredge-up into the envelopes during thermal pulses (Lattanzio & Wood 2003). In addition, our assumption is also expected to have marginal effect on integrated quantities of faint populations, as bright TP-AGB stars are statistically less frequent, or even absent. Finally, it will be shown that the details and the treatment of the physical processes at work on the TP-AGB phase, as well as their impact on synthetic colours, is still uncertain (Section 4).

The adopted colour transformations for the standard *UBVRIJHK* bands are from Castelli (1999), see also Castelli et al. (1997). To calculate integrated colours in the Hubble Space Telescope (HST) bands (WFPC2 and NICMOS systems) we adopted the colour transformations by Origlia & Leitherer (2000) based on the Bessell et al. (1998) stellar atmospheric models.

As well known the mixing length parameter (α) governs the efficiency of convection in the convective envelope of a stellar structure. The α parameter used for calculating the evolutionary tracks adopted in the present work has been calibrated in such a way that the isochrones reproduce, with the adopted colour transformations, the observed RG branch colour of GCs with the proper metallicity and age. This is evident from Fig. 2 in which our synthetic models nicely reproduce the RGB colours of the selected GCs. The α parameter needed in the present evolutionary models to obtain this agreement is $\alpha \approx 2.0$, but it's worth noticing that α is a free parameter, sensitively dependent on the chosen color transformations and on all the adopted physical inputs which affects the effective temperature of a model. Cariulo et al. (2004) showed that tracks with the same physical assumptions for metallicity up to $Z \approx 0.001$ reproduces the RGB colours of galactic GCs for the same α values, while metal-rich ($Z > 0.001$) and standard solar models require an α slightly lower (see Ciacio et al. 1997; Castellani et al. 2003).

The very low mass tracks (VLM, $M \leq 0.6 M_\odot$) are taken from Baraffe et al. (1997). The tracks have been already transformed by the authors to the observational

plane in the Johnson-Cousins system adopting the colour transformations by Allard et al. (1997), particularly suitable for low mass stars. We checked that low mass models satisfactory match, in all the available colours, the higher mass models (Fagiolini 2004). However, as already discussed by e.g. Brocato et al. (2000), VLM stars do not contribute to the photometric indices, although their contribution to the cluster mass is fundamental. Masses lower than the minimum mass for the central H ignition $\approx 0.08 M_{\odot}$, (see e.g. Baraffe et al. 1997) have been estimated do not significantly contribute to the total mass of the cluster (see e.g. Chabrier & Mera 1997), and thus they are not taken into account.

Post-AGB evolution, until the entrance in the white dwarfs (WD) cooling sequence, are not considered because the evolutionary time is too short to have a significant influence (see e.g. Blocker et al. 1997). WDs have been included in the code using evolutionary models by Salaris et al. (2000). They have been transformed by adopting the atmospheric models by Saumon & Jacobson (1999) for DA WDs, which include the treatment of the collision-induced absorption of H_2 molecules, for $T < 4000 K$. For higher temperatures the transformations of Bergeron et al. (1995) have been used. As we will discuss in the following our *standard* model adopts $6.5 M_{\odot}$ as M_{up} , (Dominguez et al. 1999). As expected, and as already noted by e.g. Angeletti et al. (1980), the contribution of the WD population to optical and NIR photometric indices is negligible although they significantly contribute to the total mass of the cluster.

The IMF of Kroupa (2002) is adopted in the mass interval $0.1 \leq M/M_{\odot} \leq 11$, unless explicitly stated otherwise. To simulate the mass distribution of stars in the synthetic CMD we use a Monte Carlo method: the position of each randomly created star in the $\log L/L_{\odot}$ vs. $\log T_e$ diagram is determined for each given age. As already discussed, the chemical composition is fixed to $Z = 0.0002$ and $Y = 0.23$.

Fig. 1 shows, as an example, synthetic CMDs (without simulation of photometric errors) for the selected chemical composition, a total absolute visual magnitude $M_V^{tot} = -6$ mag, and three different ages (500 Myr, 2 Gyr, and 11 Gyr). All the evolutionary phases described above are clearly visible.

2.2. Integrated magnitudes and colours

To compute integrated fluxes and magnitudes we assume that the integrated light from the stellar population is dominated by light emitted by its stellar component. This implies that i) no source of non-thermal emission are at work, ii) the thermal emission by interstellar gas gives no sizeable contribution to the integrated flux, and iii) the absorption from dust and gas are negligible. On this basis, the integrated flux in each photometric filter mainly depend on two quantities. The first is the flux f_i emitted by the i -th star of mass M , age t (stellar system age), lu-

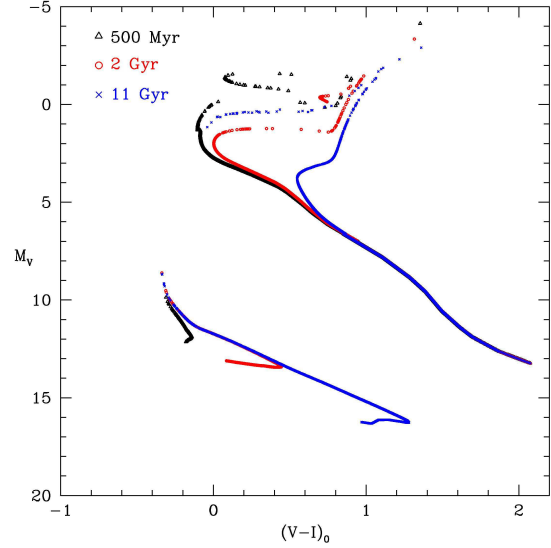


Fig. 1. Synthetic CMDs for $Z = 0.0002$, $Y = 0.23$ and three different ages: 500 Myr (black), 2 Gyr (red), and 11 Gyr (blue). For each population $M_V^{tot} = -6$ mag is adopted. The simulation of photometric errors is not included.

minosity l , effective temperature T_{eff} , and chemical composition (Y , Z):

$$f_i[l(M, t, Y, Z), T_{eff}(M, t, Y, Z), Y, Z]. \quad (3)$$

f_i is defined by the stellar evolutionary-tracks library, and by the adopted temperature-colours transformation tables.

The second quantity is $\Phi(M, N)$ which describes the number of stars with mass M in a population globally constituted of N stars with age t and chemical composition (Y , Z). It is strictly related to the IMF.

A fundamental point of our code is that the mass of each generated star is obtained by using Monte Carlo techniques, while the mass distribution is ruled by the IMF. The mass of each star is generated randomly, and its proper evolutionary line is computed by interpolating the available tracks in the mass grid. This method is crucial for poorly populated stellar systems, as we shall study in the following. It ensures to treat undersampled evolutionary phases properly; for instance NIR colours may be dominated by a handful of red giant stars (Santos & Frogel 1997; Brocato et al. 1999; Cerviño & Valls-Gabaud 2003; Raimondo et al. 2005).

In each model, stars are added until to reach a given value of the absolute visual magnitude, M_V , at any age. The mass values are generated randomly and distributed according to the chosen IMF. It is relevant to note that the random extraction of masses is fully independent from model to model even if the same input quantities (M_V , t , N , Y , Z , IMF, etc.) are assumed.

Both the previous quantities (f_i and $\Phi(M, N)$) are combined and integrated by the stellar population code to derive the total integrated flux F in a given photometric band:

$$F[N, t, Y, Z] = \sum_{i=1}^N f_i, \quad (4)$$

and the corresponding magnitudes.

3. Comparison with Galactic Globular Clusters

Before studying the general behaviour of colours and mass-to-light ratios as a function of M_V , the natural test for SSP models is to compare their predictions to the observed properties of Galactic star clusters. Three old galactic globular clusters (GGCs) have been selected for checking our capability to reproduce both the CMD morphology of each cluster and the integrated magnitudes: NGC4590 (M68), NGC7078 (M15) and NGC7099 (M30). They are all metal-poor, span a relatively wide range of the visual magnitude (Table 1), and show different Horizontal Branch morphologies. This allows us to check the effect of HB morphologies on the integrated colours in the selected bands. The $[Fe/H]$ values estimated for the three clusters are, respectively, $[Fe/H] = -2.06, -2.26, -2.12$ (Harris 1996)³, while the α -elements enhancement can be evaluated as $[\alpha/Fe] \approx 0.3$ (see, e.g. the discussion in Ferraro et al. 1999); thus we can assume $Z \approx 2 \cdot 10^{-4}$. We include M15 due to its brightness ($M_V \sim -9$), even if it is recognized as a cluster which should have undergone a gravothermal catastrophe. This results in a contraction of the cluster core while the external regions expand, with some stars escape the system. As a possible consequence of such a dynamical evolution, observational evidence of mass segregation, and of radial color gradients have been found (Bailyn et al. 1989; De Marchi & Paresce 1994; Stetson 1994).

Fig. 2 shows the observed CMDs for the selected clusters. B and V photometry comes from the HST-Snapshot Catalog by Piotto et al. (2002), except for M68 whose data are from Walker (1994). The synthetic CMD which better reproduces the observational data is over-plotted as black dots in each panel. For each cluster an age of 11 Gyr is assumed; we are not interested in a detailed calibration of the cluster ages which is far from our purpose. Results for each comparison between synthetic and observed cluster are, briefly:

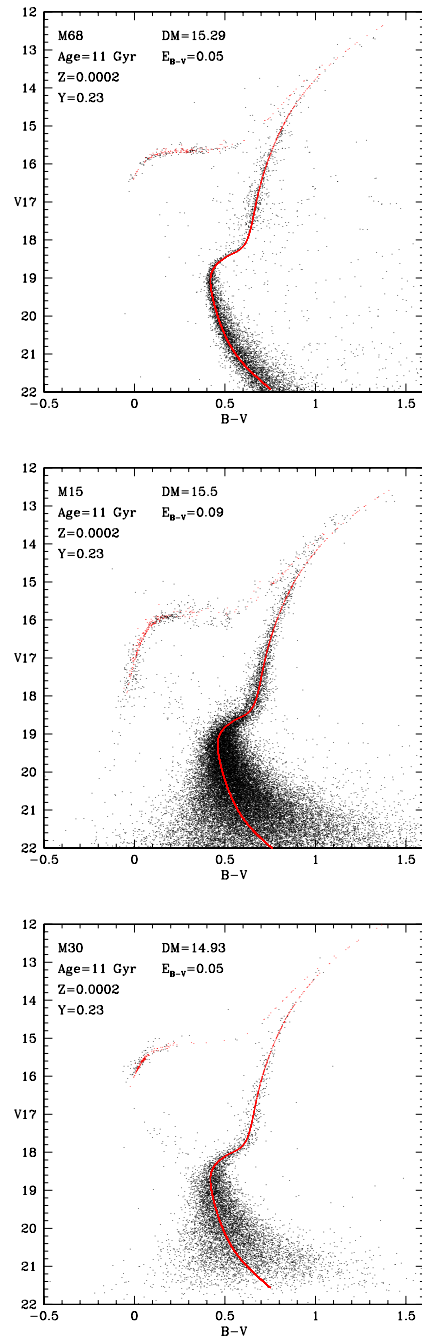


Fig. 2. Comparison between present synthetic (red dots), without the inclusion of simulated photometric errors, and the observed CMDs of the globular clusters *M68*, *M15* and *M30* (black dots). The assumed age is 11 Gyr, and the adopted chemical composition is $Z = 0.0002$ and $Y = 0.23$ (see text). The values of the distance modulus and the reddening obtained from the analysis are also indicated.

– *M68* (NGC4590): We find $(m - M)_V = 15.29$ and $E_{B-V} = 0.05$ in agreement, within the uncertainties, with the current distance modulus and reddening determinations (e.g. Harris 1996; Carretta et al. 2000; Di Criscienzo et al. 2004). The HB morphology is reproduced using $\eta_R = 0.30$ with a dispersion $\sigma_\eta = 0.08$. Due

³ www.physics.mcmaster.ca/resources/globular.html.
February 2003 version.

Table 1. Observed and theoretical integrated colours for the selected globular clusters. Values from the Harris’ catalogue are dereddened according to Reed et al. (1988). The $J - K$ near-IR colour is from Brocato et al. (1990), dereddened according to Cardelli et al. (1989). \mathcal{M}/L_V is from the compilation by Pryor & Meylan (1993).

Identity	M_V^{tot}	$U - B$	$B - V$	$V - R$	$V - I$	$J - K$	\mathcal{M}/L_V
Observations							
M68	-7.35	-0.01 ± 0.01	0.58 ± 0.03	0.43	0.88 ± 0.01	—	1.6
M15	-9.17	-0.03 ± 0.02	0.58 ± 0.01	—	0.73	0.62	2.2
M30	-7.43	-0.00 ± 0.02	0.57 ± 0.04	0.39 ± 0.02	0.82 ± 0.04	0.54	2.5
Models							
M68	-7.34 ± 0.05	0.00 ± 0.02	0.60 ± 0.02	0.42 ± 0.01	0.87 ± 0.02	0.57 ± 0.07	1.79 ± 0.07
M15	-9.18 ± 0.02	0.00 ± 0.01	0.60 ± 0.01	0.420 ± 0.003	0.89 ± 0.01	0.59 ± 0.02	1.58 ± 0.03
M30	-7.43 ± 0.05	-0.01 ± 0.01	0.59 ± 0.02	0.41 ± 0.01	0.87 ± 0.02	0.54 ± 0.05	1.76 ± 0.07

to the present uncertainties in the factors that influence the HB morphology and in the precise treatment of mass loss in the RG branch (see e.g. Lee et al. 1994; Rey et al. 2001), the tuning of the adopted value of η_R is just a way to obtain the observed HB morphology but it should not be interpreted in terms of physical parameters of the stellar cluster.

– *M15* (NGC7078): The best result is obtained by assuming $(m - M)_V = 15.50$ and $E_{B-V} = 0.09$, in agreement with current determinations on the cluster distance modulus and reddening (Harris 1996; Di Criscienzo et al. 2004; McNamara et al. 2004). The HB morphology is reproduced using $\eta_R = 0.44$ and $\sigma_\eta = 0.1$. The cluster contains one of the few planetary nebulae (PN) known in GGCs: the star K648 identified as a PN by Pease (1928), for which Alves et al. (2000) measured an apparent magnitude of $V = 14.73$.

– *M30* (NGC7099): Assuming $E_{B-V} = 0.05$ we obtain $(m - M)_V = 14.93$ in agreement with Sandquist et al. (1999). The HB morphology is reproduced using the same parameters as in Brocato et al. (2000), i.e. $\eta_R = 0.40$, and $\sigma_\eta = 0.2$.

Table 1 gives the observed integrated colours for the selected clusters, taken from the *Catalog of Parameters for Milky Way Globular Clusters* (Harris 1996)⁴ and synthetic integrated colours obtained from the present models by reproducing, within the errors, the observed total visual magnitude of each cluster. Optical observational data are de-reddened according to Reed et al. (1988) with reddening values taken from Harris (1996). To give an idea of uncertainties for the colours we report the ‘residual’ values computed by Reed (1985) which result from his homogenization procedure based on measurements of clusters colours by various authors. In some cases the availability of only one measurement prevents the determination of an uncertainty. NIR colours are from Brocato et al. (1990),

de-reddened according to Cardelli et al. (1989) with reddening values taken from Harris (1996).

Theoretical errors correspond to 1σ dispersion evaluated from 10 independent simulations. Table 1 lists: cluster NGC number (Col. 1), total absolute V magnitude (M_V^{tot} , Col. 2), integrated $U - B$, $B - V$, $V - R$, $V - I$, $V - J$ and $V - K$ colours (Cols. 3–7), and \mathcal{M}/L_V (Col. 8) from Pryor & Meylan (1993). The last values are strongly model-dependent, as stressed by the authors themselves. Hereinafter we will indicate dereddened colours as, e.g., $U - B$ instead of $(U - B)_0$.

For each cluster, numerical simulations were performed by populating the synthetic CMD until the observed M_V^{tot} of the cluster is reproduced (Sect. 2.1). Synthetic colours agree with data of all the clusters to within the uncertainties and theoretical statistical fluctuations. The only exception is the $V - I$ colour of M15 that is found to be redder than observations. The observed $V - I$ colour of this cluster is significantly bluer than that of other clusters with similar metallicity (Harris 1996). On this regard, we recall that the $V - I$ measure available is based on one photoelectric measurement only (Kron & Mayall 1960), and it is not possible to estimate the uncertainty (Reed 1985). To investigate this issue, we use VI stellar photometry by Rosenberg et al. (2000), which contains more than 90% of the cluster light ($M_V \simeq -9.1$). By adding the flux of individual stars, we derive an integrated colour $V - I \simeq 0.85$, in fair agreement with our prediction. This value is larger than the integrated value by Kron & Mayall (1960), even if it would be affected by incompleteness at the faint end of the observed luminosity function. To deeply investigate the origin of the latter inconsistency is well beyond the purpose of this paper, what we wish to point out here is to notice that the observed integrated $V - I$ colour of such a cluster, reported in Table 1, could be peculiar and then not representative of metal-poor clusters.

Additional indications may come from the analysis of M15 NIR colours. $J - K$ prediction well agrees with the value by Brocato et al. (1990) ($J - K = 0.67$, reddened), and is also consistent with data by Burstein et al. (1984) who found $J - K = 0.62$ (reddened). Interestingly, Burstein et al. (1984) also provide the observed $(V - K) =$

⁴ www.physics.mcmaster.ca/resources/globular.html.

February 2003 version. The integrated colours $U - B$ and $B - V$ are on the standard Johnson system, and $V - R$, $V - I$ on the Kron-Cousins system. The values are the simply average of results from Peterson (1993) and Reed (1985).

2.14 (reddened), that becomes $(V - K) = 1.86$ if corrected according to our reddening assumptions. By comparing this value with theory ($V - K = 2.05$), it appears that our models predict $V - K$ colour about 0.2 mag redder than observations. Unfortunately, a similar comparison cannot be done for M30 and M68, since they are not listed by Burstein et al. (1984). Instead the authors observed M92 (NGC6341), whose metallicity is estimated to be close to M15, being $[Fe/H] = -2.29$. Since M92 is as bright as $M_V = -8.20$, its colours data can be easily compared with our predictions as reported in Table 2, at age $\sim 11 - 13 \text{ Gyr}$. Interestingly, the observed optical-NIR colour $V - K = 2.13$ well agrees with our prediction, together with all the optical colours $U - B = 0.01$, $B - V = 0.61$, and $V - I = 0.86$ (from Harris’s catalog).

In conclusion, except for the peculiarity concerning M15, our models are able to properly predict the integrated colours of let’s say ‘normal’ metal-poor clusters, as confirmed by the comparison with observational data of M30, M68 (Table 1), and the additional cluster M92.

As noted above, \mathcal{M}/L values reported in the last column of Table 1 (upper section), derived using isotropic King models by Pryor & Meylan (1993), are strongly model-dependent and thus the reported values are only indicative. Moreover dynamical processes such as star evaporation (e.g. Spitzer 1987; Vesperini & Heggie 1997), may affect the total mass and the inferred IMF shape as a function of time. Observed integrated colours of the selected clusters, as well as theoretical results, indicate that they are not influenced by the HB morphology, at least in our modeled photometric bands. Shorter wavelength ultraviolet colours are expected to be more sensitive to the presence of an extended blue HB.

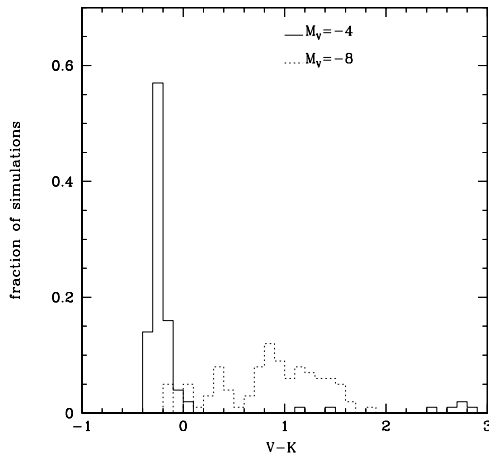


Fig. 4. $V - K$ colour distribution resulting from 100 simulations for a model with 100 Myr, $Z = 0.0002$, and $M_V^{tot} = -4$ (solid) and -8 mag (dotted).

4. Integrated colours

In this section we examine the effects on integrated colours of stochastic fluctuations for different values of the assumed total absolute visual magnitude and the effects of the still present uncertainty on the IMF shape. The Kroupa (2002) IMF is adopted for the *standard* model.

Results are presented at fixed absolute visual magnitude to aid comparisons with observational data. For these calculations the evaluation of the statistical fluctuations is fundamental. Statistical fluctuations of broadband colours as well as mass-to-light ratios have been evaluated by computing a series of 10 independent simulations for a fixed set of population’s parameters (Z , *age*, IMF, ...) at fixed M_V^{tot} , and assuming a 1σ error. When fluctuations become large, and the value above is not fully representative of colours variations, we extend the analysis up to 100 runs. This is especially the case of very poorly populated clusters ($M_V = -4$) and young ages.

The *standard* models are computed assuming: $\eta_R = 0.3$, $\sigma_\eta = 0.08$ and Kroupa’s IMF. As an example, Table 2 and 3 reports integrated colours as function of age for models with $M_V^{tot} = -8$; Johnson-Cousins colours in Tab.2 and HST colours in Tab.3. Table 2 lists from left to right: age, M_V^{tot} , integrated $(U - B)$, $(B - V)$, $(V - R)$, $(V - I)$, $(V - J)$ and $(V - K)$ colours. Table 3 reports from left to right: age, $V - F439W2$, $V - F555W2$, $V - F814W2$ for the *WFPC2* and $V - F110W1$, $V - F160W1$ for the *NICMOS* camera.

4.1. M_V^{tot} sensitivity

Our standard synthetic models are calculated for three different values of the total magnitude: $M_V^{tot} = -8$, -6 and -4 . (Note, that all the results for both broad-band colours and mass-to-light ratios for $M_V^{tot} = -6$, and -4 models are available as electronic tables at CDS).

In Fig. 3 the time evolution of selected integrated colours are shown for the two extreme cases ($M_V^{tot} = -8$, black circles, and -4 , red triangles). In general, broad-band colours become redder with age, because of the increasing fraction of cool stars in the populations. For the same reason, the $(U - B)$ colour is quite age-insensitive for age $\gtrsim 1 \text{ Gyr}$.

Within the statistical uncertainties, the mean colours at different M_V^{tot} do not show significant differences, except in a few cases at young ages, and for optical-NIR colours. This is due to the strong variation of the number of very bright red stars affecting significantly the total luminosity of the cluster. In a SSP with a total brightness as faint as $M_V^{tot} = -4$, the most of stars occupy the MS phase, and only a few (or none) red giants are present, including stars burning He in the core and stars in the double shells phase (see for example Fig. 14 in Raimondo et al. 2005). Hence, the mean $V - K$ colour (and to a less extent $V - I$) is generally bluer than in models with $M_V^{tot} = -8$, where post-MS phase is always widely populated. This effect is large in young clusters, for

Table 2. Integrated colours in the *standard* *UBVRIJHK* photometric filters for our *standard* model with $M_V^{tot} = -8$ and $Z=0.0002$.

Age (<i>Myr</i>)	M_V^{tot}	$U - B$	$B - V$	$V - R$	$V - I$	$V - J$	$V - K$
50.	-8.0 ± 0.1	-0.56 ± 0.03	-0.10 ± 0.08	-0.02 ± 0.08	0.0 ± 0.2	0.0 ± 0.3	0.1 ± 0.5
100.	-8.0 ± 0.1	-0.39 ± 0.03	0.00 ± 0.07	0.06 ± 0.07	0.2 ± 0.2	0.4 ± 0.3	0.7 ± 0.5
150.	-8.0 ± 0.1	-0.31 ± 0.02	0.01 ± 0.04	0.06 ± 0.04	0.2 ± 0.1	0.4 ± 0.2	0.7 ± 0.3
200.	-8.00 ± 0.05	-0.22 ± 0.01	0.09 ± 0.05	0.14 ± 0.05	0.4 ± 0.1	0.7 ± 0.2	1.2 ± 0.3
300.	-8.01 ± 0.09	-0.12 ± 0.02	0.14 ± 0.07	0.16 ± 0.07	0.4 ± 0.1	0.8 ± 0.2	1.3 ± 0.4
400.	-8.06 ± 0.08	-0.05 ± 0.01	0.16 ± 0.04	0.16 ± 0.04	0.41 ± 0.09	0.8 ± 0.2	1.3 ± 0.2
500.	-8.02 ± 0.05	-0.01 ± 0.01	0.19 ± 0.03	0.18 ± 0.03	0.44 ± 0.07	0.8 ± 0.1	1.3 ± 0.2
600.	-8.06 ± 0.08	0.00 ± 0.01	0.26 ± 0.03	0.22 ± 0.03	0.52 ± 0.06	1.0 ± 0.1	1.4 ± 0.2
800.	-8.03 ± 0.06	0.01 ± 0.01	0.34 ± 0.04	0.27 ± 0.03	0.62 ± 0.07	1.1 ± 0.1	1.7 ± 0.2
1000.	-7.98 ± 0.04	0.00 ± 0.01	0.36 ± 0.02	0.28 ± 0.01	0.63 ± 0.03	1.13 ± 0.06	1.6 ± 0.1
1100.	-8.02 ± 0.06	0.00 ± 0.01	0.39 ± 0.03	0.30 ± 0.02	0.66 ± 0.04	1.16 ± 0.07	1.68 ± 0.09
1500.	-8.03 ± 0.04	0.01 ± 0.01	0.41 ± 0.02	0.30 ± 0.01	0.67 ± 0.02	1.17 ± 0.04	1.70 ± 0.07
1700.	-8.00 ± 0.04	0.02 ± 0.01	0.42 ± 0.02	0.31 ± 0.01	0.68 ± 0.03	1.20 ± 0.06	1.73 ± 0.08
2000.	-7.97 ± 0.03	0.03 ± 0.01	0.44 ± 0.01	0.32 ± 0.01	0.71 ± 0.02	1.24 ± 0.04	1.78 ± 0.05
3000.	-7.98 ± 0.05	0.03 ± 0.01	0.49 ± 0.02	0.35 ± 0.01	0.75 ± 0.02	1.29 ± 0.03	1.83 ± 0.05
4000.	-8.04 ± 0.06	0.01 ± 0.01	0.53 ± 0.02	0.37 ± 0.01	0.79 ± 0.02	1.34 ± 0.03	1.89 ± 0.05
5000.	-8.01 ± 0.05	0.00 ± 0.01	0.55 ± 0.02	0.38 ± 0.01	0.80 ± 0.02	1.35 ± 0.04	1.89 ± 0.05
6000.	-8.02 ± 0.03	-0.02 ± 0.01	0.57 ± 0.01	0.39 ± 0.01	0.83 ± 0.01	1.39 ± 0.02	1.94 ± 0.03
7000.	-8.03 ± 0.04	-0.02 ± 0.01	0.60 ± 0.01	0.41 ± 0.01	0.85 ± 0.01	1.43 ± 0.02	1.99 ± 0.03
8000.	-8.00 ± 0.03	-0.02 ± 0.01	0.61 ± 0.01	0.41 ± 0.01	0.86 ± 0.01	1.44 ± 0.02	2.00 ± 0.03
9000.	-7.99 ± 0.02	-0.01 ± 0.01	0.61 ± 0.01	0.41 ± 0.01	0.87 ± 0.01	1.45 ± 0.02	2.02 ± 0.02
10000.	-7.94 ± 0.03	-0.00 ± 0.01	0.61 ± 0.01	0.42 ± 0.01	0.87 ± 0.01	1.47 ± 0.02	2.04 ± 0.03
11000.	-8.01 ± 0.04	0.00 ± 0.01	0.60 ± 0.01	0.42 ± 0.01	0.87 ± 0.01	1.46 ± 0.02	2.04 ± 0.02
12000.	-7.99 ± 0.04	0.00 ± 0.01	0.61 ± 0.01	0.42 ± 0.01	0.88 ± 0.01	1.48 ± 0.02	2.06 ± 0.03
13000.	-7.95 ± 0.05	0.01 ± 0.01	0.62 ± 0.02	0.43 ± 0.01	0.90 ± 0.02	1.51 ± 0.03	2.10 ± 0.04
14000.	-8.00 ± 0.04	0.00 ± 0.01	0.63 ± 0.01	0.43 ± 0.01	0.90 ± 0.01	1.52 ± 0.02	2.11 ± 0.03
15000.	-8.01 ± 0.04	-0.02 ± 0.01	0.62 ± 0.02	0.43 ± 0.01	0.90 ± 0.01	1.51 ± 0.03	2.10 ± 0.04

which colours are more sensitive to the cluster luminosity [see also Fig. 5 in Santos & Frogel (1997), and Fig. 8 in Brocato et al. (1999)].

To clarify this point, Fig. 4 illustrates the $V - K$ colour distribution for a SSP model with age 100 Myr; for each choice on M_V^{tot} , 100 simulations are computed. The $V - K$ colour distribution of faint clusters (solid line) shows a blue populous peak, due to the large fraction of simulations containing mainly *blue* stars, and a few sparse simulations at redder colours containing a few red giants. Consequently, the average colour is bluer than that found for brighter clusters (Fig. 3), which show a broadened colour distribution shifted towards the red side, since the probability to have a large number of red stars is higher (dotted line in Fig. 4). We emphasize that in the present paper for a given cluster age, the integrated colours at different cluster brightness are obtained by properly adding stars in all evolutionary phases according to the IMF and evolutionary time-scales (i.e. keeping fixed the proportion between the number of stars in different stages). So that, by decreasing their absolute magnitude (mass), the *natural* trend is that the cluster progressively misses post-MS stars, and due to the discreteness of stars "if an SSP is far less luminous, then there would be no post-MS stars and the integrated fluxes would be dominated by upper MS stars with little spread in color, which results in smaller color fluctuations" (Santos & Frogel 1997). The

colour behaviour described above is in agreement with Santos & Frogel (1997) and Brocato et al. (1999), while opposite to what found by Bruzual & Charlot (2003). A discussion on the nature of such a discrepancy is beyond the purpose of this paper, since it would required a deep comparison between all the assumptions adopted in all the codes (evolutionary tracks, atmospheres, etc.).

In general, for a further increase of the cluster brightness, the stochastic effects decrease, the colour distribution becomes more regular, and the standard deviation squeezes (small spread in colour).

At a given age, the size of errorbars increases as the cluster luminosity decreases; this is due to the small number of stars present in faint clusters ($M_V^{tot} = -4$, red symbols) with respect to bright ones ($M_V^{tot} = -8$, black symbols). From the figure it is evident that for all ages the statistical errors at $M_V^{tot} = -4$ are so high as to prevent precise quantitative evaluations.

The errorbars also increase from $B - V$ to $V - K$, as shown by Brocato et al. (1999). This last finding is related again to the expected small number of post-MS stars shining in the infrared wavelengths, especially in case of low-luminosity clusters ($M_V^{tot} = -4$). Moreover, in faint clusters it may happen that giant stars are not present in each of the simulations we computed at fixed age, being their appearance highly driven by stochastic phenomena. At fixed total magnitude the *intrinsic* uncertainty lowers

Table 3. As in Table 2 but for WFPC2 (first three columns), and NICMOS1 (last two columns) photometric bands.

Age (<i>Myr</i>)	$V - 439W(2)$	$V - F555W(2)$	$V - F814W(2)$	$V - F110W(1)$	$V - F160W(1)$
50.	0.09 ± 0.08	0.009 ± 0.005	0.0 ± 0.2	0.0 ± 0.3	0.0 ± 0.5
100.	-0.01 ± 0.08	0.002 ± 0.005	0.2 ± 0.2	0.3 ± 0.3	0.6 ± 0.5
150.	-0.02 ± 0.03	0.000 ± 0.002	0.2 ± 0.1	0.3 ± 0.1	0.6 ± 0.3
200.	-0.11 ± 0.05	-0.006 ± 0.003	0.3 ± 0.1	0.6 ± 0.2	1.1 ± 0.3
300.	-0.15 ± 0.07	-0.009 ± 0.004	0.4 ± 0.1	0.6 ± 0.2	1.2 ± 0.4
400.	-0.18 ± 0.05	-0.011 ± 0.003	0.4 ± 0.09	0.6 ± 0.1	1.2 ± 0.2
500.	-0.21 ± 0.04	-0.013 ± 0.002	0.42 ± 0.07	0.7 ± 0.1	1.2 ± 0.2
600.	-0.28 ± 0.04	-0.018 ± 0.002	0.50 ± 0.06	0.8 ± 0.1	1.3 ± 0.1
800.	-0.38 ± 0.04	-0.023 ± 0.002	0.60 ± 0.07	0.9 ± 0.1	1.5 ± 0.1
1000.	-0.40 ± 0.02	-0.024 ± 0.001	0.61 ± 0.03	0.93 ± 0.05	1.53 ± 0.08
1100.	-0.43 ± 0.03	-0.025 ± 0.001	0.63 ± 0.04	0.99 ± 0.06	1.57 ± 0.10
1500.	-0.45 ± 0.02	-0.026 ± 0.001	0.64 ± 0.02	0.97 ± 0.04	1.58 ± 0.06
1700.	-0.46 ± 0.02	-0.027 ± 0.001	0.66 ± 0.03	0.99 ± 0.05	1.61 ± 0.08
2000.	-0.49 ± 0.01	-0.028 ± 0.001	0.68 ± 0.02	1.03 ± 0.03	1.66 ± 0.05
3000.	-0.55 ± 0.02	-0.031 ± 0.001	0.72 ± 0.02	1.07 ± 0.03	1.71 ± 0.05
4000.	-0.60 ± 0.02	-0.033 ± 0.001	0.76 ± 0.02	1.12 ± 0.03	1.77 ± 0.04
5000.	-0.61 ± 0.02	-0.033 ± 0.001	0.76 ± 0.02	1.11 ± 0.03	1.75 ± 0.04
6000.	-0.65 ± 0.01	-0.035 ± 0.001	0.89 ± 0.01	1.17 ± 0.02	1.82 ± 0.02
7000.	-0.67 ± 0.02	-0.035 ± 0.001	0.81 ± 0.02	1.18 ± 0.03	1.84 ± 0.04
8000.	-0.69 ± 0.01	-0.036 ± 0.001	0.83 ± 0.01	1.21 ± 0.02	1.88 ± 0.03
9000.	-0.70 ± 0.02	-0.036 ± 0.001	0.83 ± 0.01	1.22 ± 0.02	1.90 ± 0.03
10000.	-0.70 ± 0.01	-0.036 ± 0.001	0.84 ± 0.01	1.23 ± 0.02	1.92 ± 0.03
11000.	-0.69 ± 0.01	-0.035 ± 0.001	0.84 ± 0.02	1.23 ± 0.01	1.91 ± 0.02
12000.	-0.69 ± 0.01	-0.035 ± 0.001	0.85 ± 0.01	1.25 ± 0.02	1.94 ± 0.03
13000.	-0.71 ± 0.02	-0.036 ± 0.001	0.86 ± 0.01	1.27 ± 0.02	1.97 ± 0.03
14000.	-0.72 ± 0.01	-0.036 ± 0.001	0.87 ± 0.01	1.28 ± 0.02	1.98 ± 0.03
15000.	-0.72 ± 0.02	-0.036 ± 0.001	0.87 ± 0.02	1.28 ± 0.02	1.97 ± 0.04

with age, also because a larger number of stars is needed to reach the given total magnitude.

4.2. IMF variations

To evaluate the effect of IMF variations on integrated colours we changed the Kroupa (2002) IMF exponent (x) within the estimated uncertainty for masses $M > 0.5 M_{\odot}$. In Fig. 5 models with $M_V^{tot} = -8$ calculated with the lower, central and upper value of the IMF exponent are plotted in selected pass-bands; the corresponding data tables are available as electronic tables at CDS.

As obtained for metal-rich models investigated in previous papers (see e.g. Maraston 1998; Brocato et al. 2000; Yi 2003; Bruzual & Charlot 2003), we find that colours variations are negligible also for very low-metallicity models, at least in the range of exponent investigated here, being the colours variations well within the intrinsic uncertainty, for both values of the brightness of the cluster ($M_V^{tot} = -4$ mag and -8). The errorbars behavior is similar to what described above: colour fluctuations increase from optical-optical to optical-NIR colours and for ages $\lesssim 1$ Gyr.

Changing the distribution of very low mass stars ($M \leq 0.5 M_{\odot}$) has negligible effects on photometric indices whatever the total visual magnitude, as already

shown by Brocato et al. (2000) for ages greater than 5 Gyr. In poorly populated clusters ($M_V^{tot} = -4$ mag) as in the richest ones ($M_V^{tot} = -8$ mag), reducing the number of stars with $M < 0.5 M_{\odot}$ does not affect the integrated colours since the contribution of these stars to the total V light is only of the order of few percent (Brocato et al. 2000). The contribution of such stars slightly increases with age, but it remains comparable to the statistical errors even at the oldest ages (at least in the range explored here).

4.3. Comparison with previous works

Table 4 summarizes the main ingredients used by various authors in their synthesis code, and Fig. 6 compares the time-evolution of $B - V$ and $V - K$ colours of the present work with similar recent results available in the literature. In the figure our models are plotted with 1σ intrinsic error, while other authors do not estimate the colours statistical errors, except for Brocato et al. (2000). If colours are not available for exactly the same metallicity value adopted in the present work ($Z = 0.0002$), the two closest Z values are plotted. The models referred as Anders & Fritze-v. Alvensleben (2003) are the ones of the quoted paper, updated concerning emission lines by private communication (see also Schulz et al. 2002).

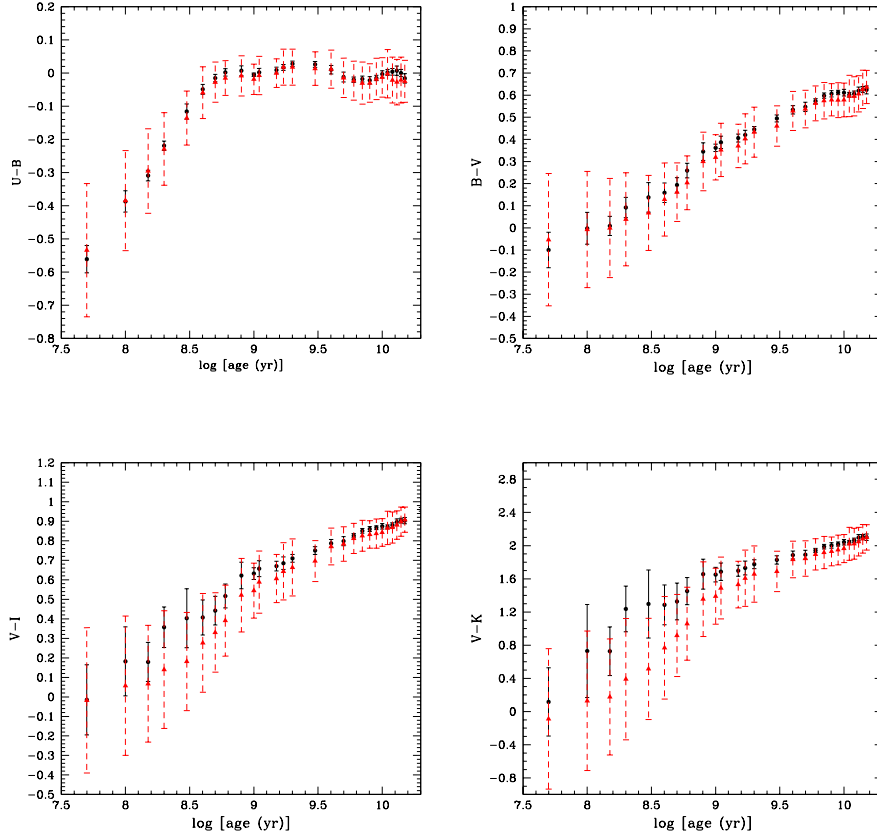


Fig. 3. Time evolution of selected integrated colours in the standard *UBVR IJHK* filters for models with $M_V^{tot} = -4$ (red triangles, dashed lines) and $M_V^{tot} = -8$ (black points, solid lines). For each model 1σ colour dispersion is reported, see text.

The present predictions well agree with those by Brocato et al. (2000). There is also a general good agreement with Kurth et al. (1999), and Bruzual & Charlot (2003), both based on *Padua 1994* stellar evolutionary tracks (see the quoted papers for the detailed list of references). Differences can be found in the age range $8.6 \lesssim \log \text{age}(\text{yr}) \lesssim 9$ for optical-NIR colours, possibly due to the treatment of the AGB and TP-AGB phases. Girardi et al. (2000) and Anders & Fritze-v. Alvensleben (2003) predict redder colours than all the other authors for $\text{age} \gtrsim 100$ Myr, as well as Zhang et al. (2002) for $\text{age} \gtrsim 3$ Gyr. Differently from the others, both Maraston (2005) and our models are based on no-overshooting tracks. Nevertheless, while the present $B - V$ colours well agree with Maraston’s models at all ages in common, $V - K$ predictions are bluer than those by Maraston (2005) at ages younger than $\simeq 3$ Gyr.

Fig. 6 shows that the $B - V$ and $V - K$ predictions from different authors agree within 0.1 mag at $\log \text{age} \gtrsim 9.3$. Large model-to-model differences arise at young and intermediate ages, when the contribution of AGB and TP-AGB stars to the total flux is high, especially in the NIR bands (see for a discussion Maraston 1998; Girardi & Bertelli 1998). This has a direct consequence on predicted colours,

since a large variety of stellar ingredients and prescriptions are used to simulate these phases. Temperature-colours relations, mass-loss prescriptions, and analytical description of the TP evolution all affect the photometric properties of such kind of stars, thus it is not straightforward to individuate a single origin (or multiple ones) to explain differences shown in Fig. 6 in the intermediate-age range.

For instance, mass-loss processes affecting TP-AGB stars are one of the physical mechanisms largely affecting the TP-AGB stars evolution. However, the effect of mass loss on the observational properties of TP stars are largely unknown to date. To give an indication on how mass-loss may affects colour predictions, we made numerical experiments by computed integrated colours in the extreme case when no TP-AGB stars are present in the population, to mimic in such a way a very efficient mass-loss rate (see also Maraston 1998). As expected, the effect is larger for intermediate-age populations, and in the optical-NIR colours. The $V - K$ colour becomes bluer than the *standard* value by ~ 0.5 mag at $\text{age} = 500$ Myr, and the $B - V$ colour decreases only by 0.06 mag at the same age. This effect tends to vanish by increasing the age. On the other hand, if we lower the mass-loss efficiency with respect to our *standard* assumption (BH) by

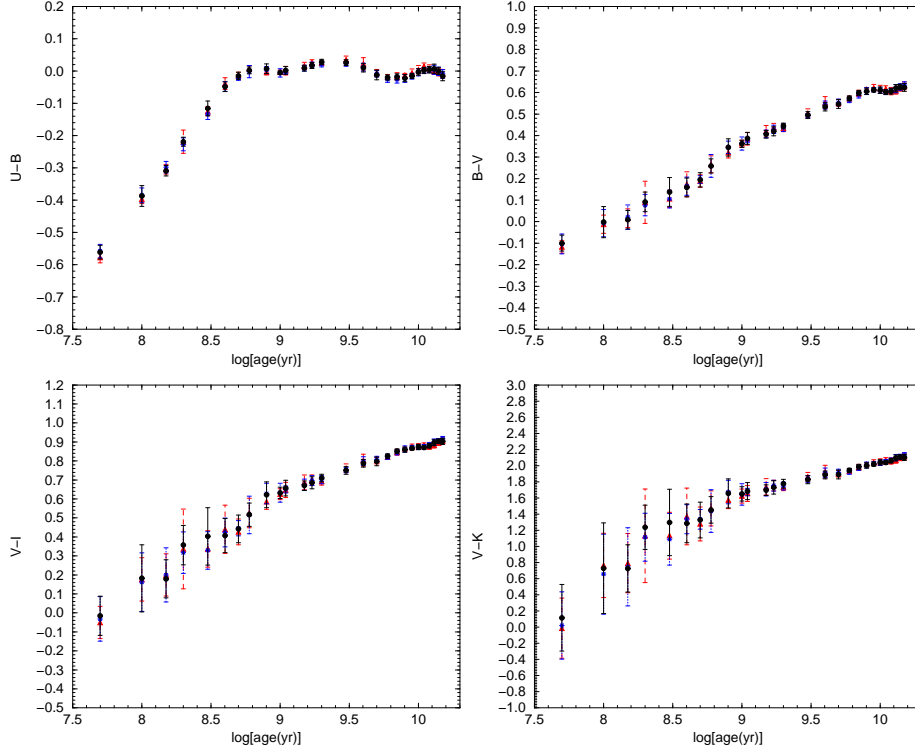


Fig. 5. Time evolution of selected integrated colours for SSPs with $M_V^{tot} = -8$ calculated with the lower, central and upper value for the Kroupa (2002) IMF exponent (α) for $M \geq 0.5 M_\odot$. Black dots indicate our reference model ($\alpha = 2.3$), red triangles indicate models with $\alpha = 2.0$ and blue stars models with $\alpha = 2.6$.

using a Reimers' law with η of the order of 1, and $V - K$ colours redder than our 'standard' models are obtained. As a consequence the colour decline at age corresponding to the appearance of He-core degenerate stars is more evident ($t \sim 1 \text{ Gyr}$), similarly to what obtained by Maraston (2005), and by Raimondo et al. (2005) for surface brightness fluctuation colours.

5. Mass-to-light ratio

Table 6 lists our predictions for the mass-to-light ratio (\mathcal{M}/L) in various photometric bands as function of age for $M_V^{tot} = -8$; similar tables for $M_V^{tot} = -6$ and $M_V^{tot} = -4$ are available at CDS.

The total mass \mathcal{M} includes all the evolving stars up to the AGB tip ($M \geq 0.1 M_\odot$) and WDs. Stars with mass higher than $M_{up} = 7 M_\odot$ are assumed to leave a neutron star (NS) as a remnant. To evaluate the maximum mass fraction of NS we set the neutron star mass at its upper limit ($\approx 2 M_\odot$, see e.g. Bombaci et al. 2004), and we choose high cluster age ($\approx 12 \text{ Gyr}$); we found that the NS mass fraction constitutes at maximum few percent of the cluster mass in agreement with the calculations by Vesperini & Heggie (1997) who found an upper value of $\approx 1\%$. The contribution of massive black holes to the total mass depends on assumption on the mass of the remnant and IMF (Maraston 2005). By using the same prescriptions on black holes mass as Maraston (2005), we

estimated that for a Kroupa IMF the mass fraction of both neutron stars and black holes does not exceed 5-10%.

In this paper, the \mathcal{M}/L values are calculated without taking into account any dynamical processes, e.g. evaporation of stars due to two body relaxation or disk shocking (see e.g. Spitzer 1987; Vesperini & Heggie 1997; Boily et al. 2005). A treatment of these phenomena is beyond the scope of this work; N-body simulations showing the effects of this processes on the total mass and IMF shape as a function of time, and on the galactocentric distance of the cluster can be found in e.g. Vesperini & Heggie (1997). We only note that since stellar evaporation is more efficient for low mass stars, one expects a flattening of the IMF as the dynamical evolution of a cluster proceeds. Evaluations of the mass fraction of WDs expected to be lost from clusters due to dynamical evaporation can be found in Vesperini & Heggie (1997) (see also Fellhauer et al. 2003; Hurley & Shara 2003). The presence of binary stars is not taken into account as well; the lack of information about the binary frequency, the distribution of binaries of different mass ratios, the separation of the components, and the occurrence of explosion of novae and supernovae prevents a quantitative treatment of this phenomenon. An attempt to include binary systems in population synthesis models has recently been presented by Zhang et al. (2005).

In Fig. 7 we show the influence of VLM stars ($M \leq 0.6 M_\odot$) and WDs on the \mathcal{M}/L , L is the bolometric luminosity in solar units, at fixed absolute visual magnitude

Table 4. The physical ingredients adopted in the models plotted in Fig.6. The quoted values for the overshooting (OS) efficiency, expressed in unit of pressure-scale-height above the Schwarzschild convective border, are only indicative because different sets of evolutionary tracks adopt different prescriptions for the overshooting mechanisms and for the minimum mass at which the overshooting is fully efficient (see the related papers for more details); Y=YES; N=NO. WD indicates if white dwarfs are included in the calculations; \mathcal{M}/L if mass-to-light ratio values are available. In the paper by Kurth et al. (1999) the normalization procedure is not described. In the paper by Anders & Fritze-v. Alvensleben (2003), the SSPs have been evolved to the selected ages starting with an initial stellar mass of $10^6 M_\odot$; the adopted value for M_{up} is not specified. ¹ Detailed information on the adopted evolutionary tracks can be found in the paper quoted in Col. 1. ² Latest version available on the web, see Maraston (2005). ³ Synthetic models are also calculated for Salpeter (1955) IMF. ⁴ See discussion in Maraston (2005). ⁵ Carbon stars included.

Authors	Evolutionary Tracks	Stellar Spectral Library	IMF	Normalization	Thermal Pulses	OS [H _p]	M_{up} [M_\odot]	WD	\mathcal{M}/L
Kurth et al. (1999)	Padua Lib. 1994 ¹ + Chabrier & Baraffe (1997)	Lejeune et al. (1997, 1998)	Salpeter (1955)	—	N	≈ 0.2	5	N	N
Brocato et al. (2000)	Frascati Lib. 1991-2000 ¹	Kurucz (1993) Castelli et al. (1997)	Scalo (1986)	N. of stars & M_V^{tot}	Groenewegen & de Jong (1993)	N	5	Y	N
Girardi et al. (2000)	Padua Lib. 1994-2000 ¹	Kurucz (1992)	Salpeter (1955)	$1 M_\odot$	Groenewegen & de Jong (1993) + Marigo (1998)	≈ 0.25	5	Y	N
Zhang et al. (2002)	Pols et al. (1998)	Lejeune et al. (1997, 1998)	Kroupa et al. (1993)	$1 M_\odot$	Vassiliadis & Wood (1993)	$0.22 \div 0.4$	5	Y	N
Anders & Fritze-v. Alvensleben (2003)	Padua Lib. 1994-2000 ¹ + Chabrier & Baraffe (1997)	Lejeune et al. (1997, 1998)	Salpeter (1955)	Initial cluster mass $1.6 \cdot 10^9 M_\odot$	Groenewegen & de Jong (1993)	≈ 0.25	-	Y	Y
Bruzual & Charlot (2003)	Padua Lib. 1994 ¹ + Baraffe (1998)	Westera et al. (2002)	Chabrier (2003)	$1 M_\odot$	Vassiliadis & Wood ⁵ (1993)	≈ 0.2	5	Y	Y
Maraston (2005)	Cassisi et al. (2000) ¹	Lejeune et al. (1998) ²	Kroupa (2001) ³	$1 M_\odot$	Renzini (1992) ^{4,5}	N	8.5	Y	Y
Present work	Pisa Lib. 2004 + Baraffe et al. (1997)	Castelli (1999)	Kroupa (2002)	M_V^{tot}	Wagenhuber & Groenewegen (1998)	N	6.5	Y	Y

($M_V = -8$). As already known, VLM and WDs provide a nearly negligible contribution to the total luminosity (see for example Maraston 1998), while give a significative contribution to the total mass. Fig. 7 shows that the fraction of low mass stars and white dwarfs increases with the cluster age (see also Maraston 1998). Note that, since the simulations are performed at fixed absolute visual magnitude, the total mass of the cluster varies with age, as shown in Fig. 8, where we plot the case of $M_V = -8$. This is because as the age increases the mass of the typical star in the cluster decreases.

Changing M_{up} affects the number of stars cooling as WDs, or in other words the mass fraction locked as WDs, and thus the cluster total mass. Different input ingredients of stellar evolutionary tracks, as e.g. the neutrino energy losses in the core, lead to different predictions of M_{up} at fixed metallicity, see e.g. Tornambe & Chieffi (1986, $M_{up} = 5.7 M_\odot$), Pols et al. (1998, $M_{up} = 5 M_\odot$), Dominguez et al. (1999, $M_{up} = 6.5 M_\odot$), Cariulo et al. (2004, $M_{up} = 5 \div 6 M_\odot$). We explore the effect of changing M_{up} . We find that increasing M_{up} from 5 up to $7 M_\odot$ does not cause variations in the mass-to-light ratios, at least for the adopted IMF. Even pushing M_{up} up to $10 M_\odot$ does not cause sensitive change in the mass-to-light ratios (Table 5).

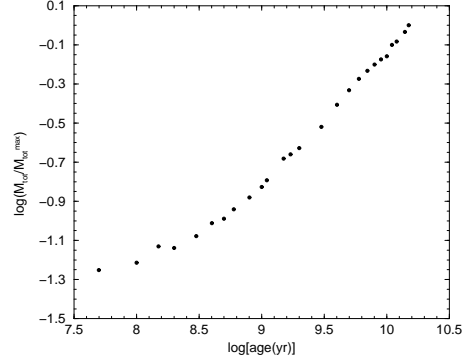


Fig. 8. Time behaviour of the logarithm of the cluster total mass needed to reach $M_V^{tot} = -8$ normalized to the maximum value, as a function of age.

5.1. M_V^{tot} sensitivity

Fig. 9 shows the time evolution of \mathcal{M}/L ratio in selected passbands for *standard* models with $M_V^{tot} = -8$ (Table 6) and -4 mag. The corresponding data tables for other passbands and for the case of $M_V^{tot} = -6$ are available at CDS. Note that the mass-to-light ratios generally increase with age independently of the photometric band, because the total mass increases. This result is similar to what obtained by other authors, who do not keep constant the lu-

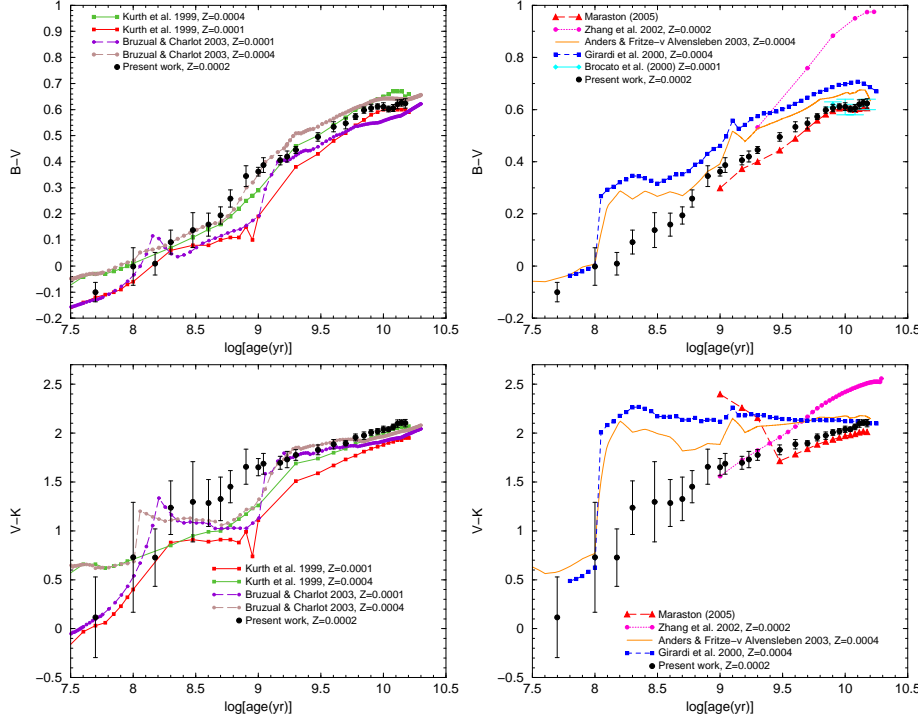


Fig. 6. Comparison between theoretical integrated colours ($B-V$, upper panels; $V-K$, lower panels) from recent papers: present models (black dots); Kurth et al. (1999, red $Z=0.0001$, green $Z=0.0004$ squares, solid line), Brocato et al. (2000, cyan dots), Anders & Fritze-v. Alvensleben (2003, orange solid line), Girardi et al. (2000, blue squares, short-dashed line), Zhang et al. (2002, pink circles, dotted line), Bruzual & Charlot (2003, violet $Z=0.0001$, brown $Z=0.0004$ circles, dashed line). Maraston (2005, red triangles, dashed line).

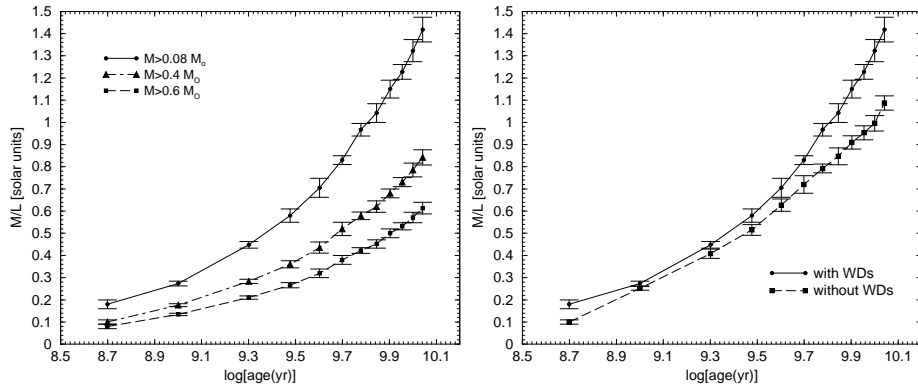


Fig. 7. Left panel: Fraction of very low mass stars ($M \leq 0.6 M_{\odot}$) that contribute to the mass–luminosity ratio (\mathcal{M}/L) (in solar units) as a function of the age for $M_V^{tot} = -8$. Filled circles represent our *standard* model in which all masses with $M \geq 0.08 M_{\odot}$ are included; the effect of considering only stars with $M \geq 0.4 M_{\odot}$ (filled triangles) or $M \geq 0.6 M_{\odot}$ (filled squares) is analyzed separately. Right panel: as in the left panel, but when the WD population is (filled circles, *standard* model) or is not (filled squares) included.

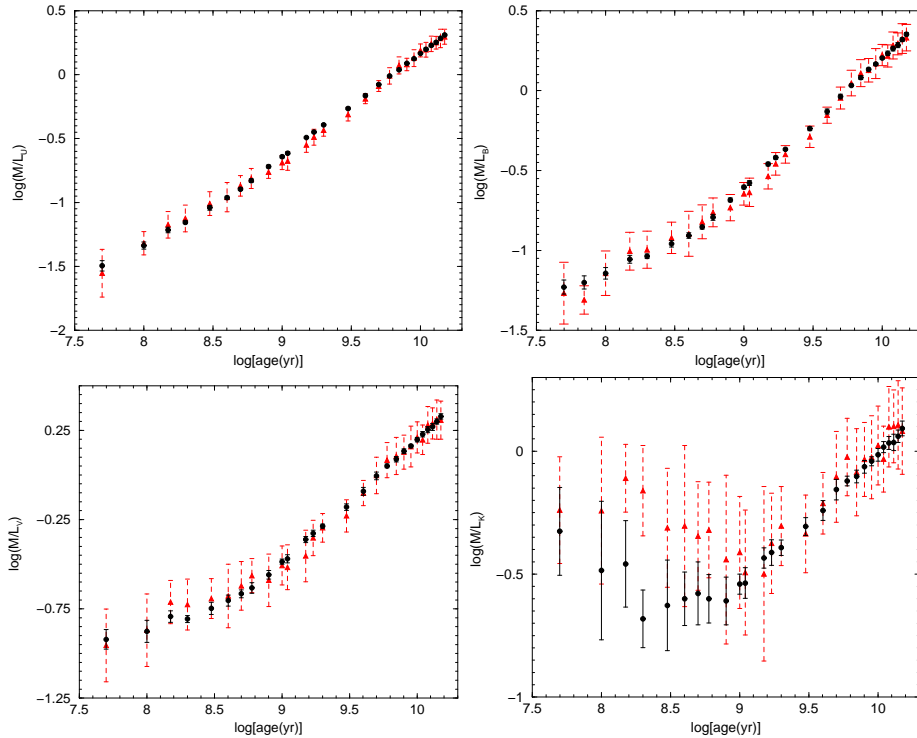
minosity L_V (see e.g. Bruzual & Charlot 2003; Maraston 2005).

The only effect of changing the absolute magnitude from $M_V = -8$ to -4 on mass-to-light ratios in the optical bands is to increase the intrinsic uncertainties. On the contrary, other than this effect mass-to-light ratios in the NIR bands suffer a larger scatter due to the decrease of red giants contributors to the total NIR luminosity, as shown in the right lower panel of the figure for K -band.

Since M_V^{tot} is fixed, the behaviour of (\mathcal{M}/L_V) as a function of the age reflects the trend of the cluster mass (Fig. 8); it is quite linear for ages $\geq 1 \text{ Gyr}$ in all pass-bands indicating it is driven by the grown of the total mass. For ages $\leq 1 \text{ Gyr}$ NIR colours are flatter than the optical (U, B, V) ones due to the increase of the infrared luminosity following the develop of an extended asymptotic giant branch. We also find a dimming in \mathcal{M}/L_K at the age corresponding to the AGB phase-transition con-

Table 5. Mass-to-light ratios for selected ages in several photometric passbands from our *standard* model with different assumptions of M_{up} .

	M/L_V	M/L_U	M/L_B	M/L_R	M/L_I	M/L_J	M/L_K
$M_{up} = 5 M_\odot$							
500 <i>Myr</i>	0.21 ± 0.01	0.126 ± 0.003	0.139 ± 0.004	0.25 ± 0.02	0.28 ± 0.04	0.28 ± 0.06	0.26 ± 0.08
800 <i>Myr</i>	0.28 ± 0.02	0.194 ± 0.007	0.210 ± 0.008	0.31 ± 0.03	0.31 ± 0.04	0.29 ± 0.05	0.25 ± 0.06
3 <i>Gyr</i>	0.66 ± 0.03	0.55 ± 0.01	0.58 ± 0.02	0.67 ± 0.03	0.64 ± 0.03	0.58 ± 0.04	0.50 ± 0.04
10 <i>Gyr</i>	1.55 ± 0.04	1.45 ± 0.02	1.58 ± 0.03	1.47 ± 0.04	1.33 ± 0.05	1.15 ± 0.05	0.95 ± 0.05
$M_{up} = 6.5 M_\odot$							
500 <i>Myr</i>	0.22 ± 0.01	0.127 ± 0.003	0.140 ± 0.004	0.26 ± 0.02	0.28 ± 0.03	0.29 ± 0.06	0.26 ± 0.08
800 <i>Myr</i>	0.28 ± 0.01	0.191 ± 0.005	0.207 ± 0.006	0.30 ± 0.02	0.30 ± 0.03	0.28 ± 0.05	0.25 ± 0.06
3 <i>Gyr</i>	0.66 ± 0.03	0.55 ± 0.01	0.58 ± 0.02	0.67 ± 0.03	0.64 ± 0.04	0.58 ± 0.04	0.49 ± 0.04
10 <i>Gyr</i>	1.58 ± 0.05	1.47 ± 0.02	1.60 ± 0.03	1.49 ± 0.05	1.36 ± 0.06	1.17 ± 0.06	0.97 ± 0.06
$M_{up} = 10 M_\odot$							
500 <i>Myr</i>	0.22 ± 0.01	0.130 ± 0.002	0.143 ± 0.003	0.26 ± 0.02	0.28 ± 0.04	0.28 ± 0.06	0.26 ± 0.08
800 <i>Myr</i>	0.29 ± 0.01	0.199 ± 0.005	0.214 ± 0.005	0.31 ± 0.02	0.31 ± 0.03	0.29 ± 0.05	0.25 ± 0.05
3 <i>Gyr</i>	0.68 ± 0.03	0.56 ± 0.01	0.60 ± 0.02	0.69 ± 0.04	0.66 ± 0.04	0.60 ± 0.04	0.51 ± 0.05
10 <i>Gyr</i>	1.58 ± 0.05	1.48 ± 0.02	1.61 ± 0.04	1.49 ± 0.06	1.35 ± 0.06	1.16 ± 0.06	0.96 ± 0.06

**Fig. 9.** Time behaviour of the M/L ratio (in solar units) for selected passbands (U, B, V, K). For each model 1σ dispersion is shown. Red triangles (dashed line) indicate models with $M_V^{tot} = -4$, and black dots (continuous line) models with $M_V^{tot} = -8$.

firming the result found by Maraston (2005) for higher metallicity.

Finally, Fig. 10 compares the present values with the ones by Bruzual & Charlot (2003), Anders & Fritze-v.Alvensleben (2003), and Maraston (2005) in two photometric bands, namely B and K . Concerning the B -band, the agreement with Bruzual & Charlot (2003) and Maraston (2005) is

very satisfactory, while Anders & Fritze-v.Alvensleben (2003) predict slightly higher values at $\log age \gtrsim 8.5$.

A more complex behaviour is shown by M/L_K : at $\log age \gtrsim 9.3$ the M/L_K is independent of the model, while model-dependent at younger ages. This reflects the great uncertainties in simulating the AGB phase we have already discussed for colours.

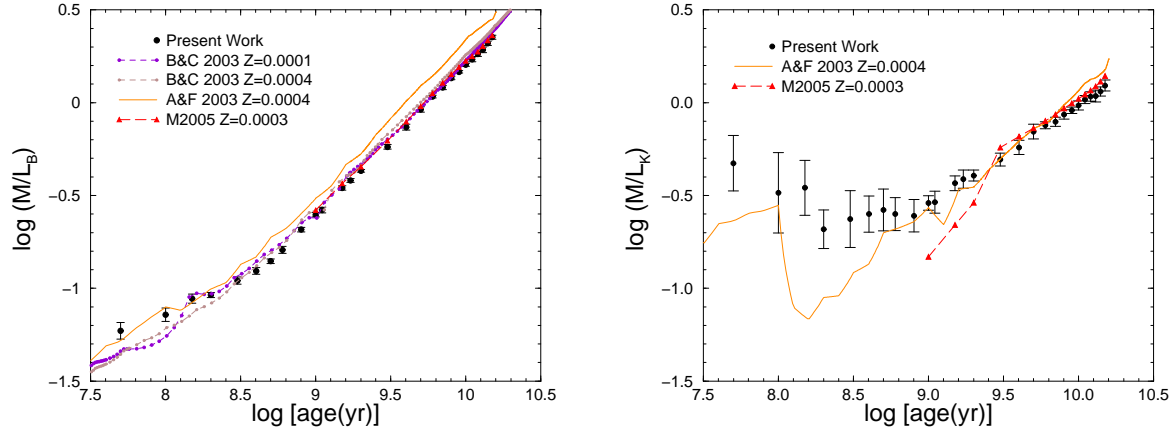


Fig. 10. Time evolution of \mathcal{M}/L_B (left panel) and \mathcal{M}/L_K (right panel) in our reference model (black dots) compared with the Bruzual & Charlot (2003, B&C 2003) for models with $Z = 0.0001$ (violet dashed line), and $Z = 0.0004$ (brown dashed line), Anders & Fritze-v. Alvensleben (2003, A&F 2003) models (orange solid line), and Maraston (2005, M2005) for $Z = 0.0003$ (red triangles, dashed line). The IMF adopted by various authors are reported in Table 4.

Table 6. Theoretical \mathcal{M}/L as a function of the age in different photometric bands (solar units) obtained for *standard* models with $M_V^{tot} = -8$.

Age (Myr)	\mathcal{M}/L_V	\mathcal{M}/L_U	\mathcal{M}/L_B	\mathcal{M}/L_R	\mathcal{M}/L_I	\mathcal{M}/L_J	\mathcal{M}/L_K
50.	0.12 ± 0.01	0.032 ± 0.003	0.06 ± 0.01	0.17 ± 0.02	0.24 ± 0.05	0.4 ± 0.1	0.5 ± 0.2
100.	0.13 ± 0.02	0.046 ± 0.003	0.07 ± 0.01	0.18 ± 0.04	0.22 ± 0.07	0.3 ± 0.1	0.3 ± 0.2
150.	0.16 ± 0.01	0.061 ± 0.003	0.088 ± 0.005	0.21 ± 0.02	0.26 ± 0.04	0.33 ± 0.08	0.3 ± 0.1
200.	0.16 ± 0.01	0.070 ± 0.002	0.092 ± 0.003	0.19 ± 0.01	0.22 ± 0.03	0.23 ± 0.05	0.21 ± 0.06
300.	0.18 ± 0.01	0.091 ± 0.004	0.110 ± 0.005	0.22 ± 0.03	0.24 ± 0.05	0.25 ± 0.08	0.24 ± 0.10
400.	0.20 ± 0.01	0.109 ± 0.003	0.124 ± 0.005	0.24 ± 0.02	0.26 ± 0.04	0.27 ± 0.05	0.25 ± 0.06
500.	0.22 ± 0.01	0.127 ± 0.003	0.140 ± 0.004	0.25 ± 0.02	0.28 ± 0.03	0.29 ± 0.06	0.26 ± 0.08
600.	0.23 ± 0.02	0.148 ± 0.005	0.16 ± 0.01	0.27 ± 0.02	0.28 ± 0.03	0.28 ± 0.05	0.25 ± 0.06
800.	0.28 ± 0.01	0.191 ± 0.005	0.21 ± 0.01	0.30 ± 0.02	0.30 ± 0.03	0.28 ± 0.05	0.25 ± 0.05
1000.	0.33 ± 0.01	0.23 ± 0.01	0.25 ± 0.01	0.35 ± 0.01	0.35 ± 0.02	0.33 ± 0.02	0.29 ± 0.03
1100.	0.34 ± 0.02	0.24 ± 0.01	0.26 ± 0.01	0.36 ± 0.03	0.36 ± 0.03	0.33 ± 0.04	0.29 ± 0.04
1500.	0.43 ± 0.02	0.32 ± 0.01	0.35 ± 0.01	0.46 ± 0.02	0.45 ± 0.03	0.42 ± 0.03	0.37 ± 0.03
1700.	0.47 ± 0.02	0.36 ± 0.01	0.38 ± 0.01	0.49 ± 0.03	0.48 ± 0.03	0.45 ± 0.04	0.39 ± 0.05
2000.	0.52 ± 0.01	0.40 ± 0.01	0.43 ± 0.01	0.53 ± 0.02	0.52 ± 0.02	0.47 ± 0.03	0.40 ± 0.03
3000.	0.66 ± 0.03	0.54 ± 0.01	0.59 ± 0.02	0.67 ± 0.03	0.64 ± 0.04	0.58 ± 0.04	0.49 ± 0.04
4000.	0.81 ± 0.04	0.69 ± 0.02	0.74 ± 0.03	0.80 ± 0.05	0.75 ± 0.05	0.68 ± 0.05	0.57 ± 0.05
5000.	0.99 ± 0.05	0.84 ± 0.02	0.92 ± 0.03	0.97 ± 0.06	0.91 ± 0.06	0.82 ± 0.07	0.70 ± 0.07
6000.	1.12 ± 0.03	0.97 ± 0.01	1.08 ± 0.02	1.09 ± 0.03	1.01 ± 0.03	0.89 ± 0.03	0.76 ± 0.03
7000.	1.22 ± 0.04	1.09 ± 0.02	1.21 ± 0.03	1.17 ± 0.05	1.08 ± 0.05	0.94 ± 0.05	0.80 ± 0.05
8000.	1.36 ± 0.04	1.22 ± 0.02	1.36 ± 0.03	1.30 ± 0.05	1.18 ± 0.05	1.03 ± 0.05	0.86 ± 0.05
9000.	1.45 ± 0.03	1.33 ± 0.02	1.47 ± 0.02	1.38 ± 0.04	1.26 ± 0.04	1.09 ± 0.04	0.91 ± 0.04
10000.	1.58 ± 0.05	1.47 ± 0.02	1.60 ± 0.03	1.49 ± 0.05	1.36 ± 0.06	1.17 ± 0.06	0.97 ± 0.06
11000.	1.69 ± 0.06	1.58 ± 0.04	1.71 ± 0.05	1.61 ± 0.06	1.46 ± 0.06	1.25 ± 0.06	1.04 ± 0.05
12000.	1.80 ± 0.07	1.69 ± 0.04	1.83 ± 0.06	1.70 ± 0.07	1.54 ± 0.07	1.31 ± 0.07	1.08 ± 0.07
13000.	1.86 ± 0.09	1.78 ± 0.05	1.93 ± 0.07	1.74 ± 0.09	1.57 ± 0.09	1.33 ± 0.09	1.08 ± 0.08
14000.	1.99 ± 0.07	1.92 ± 0.04	2.09 ± 0.06	1.86 ± 0.07	1.67 ± 0.07	1.41 ± 0.07	1.15 ± 0.07
15000.	2.13 ± 0.07	2.04 ± 0.03	2.25 ± 0.06	1.99 ± 0.08	1.78 ± 0.09	1.51 ± 0.09	1.24 ± 0.09

5.2. IMF variations

To evaluate the effect of the IMF shape on \mathcal{M}/L we changed the IMF exponents within the estimated uncer-

tainty (Kroupa 2002). Fig. 11 and Fig. 12 show the effect of changing the IMF exponents with respect to the Kroupa's formulation for masses higher and lower than $0.5 M_\odot$, re-

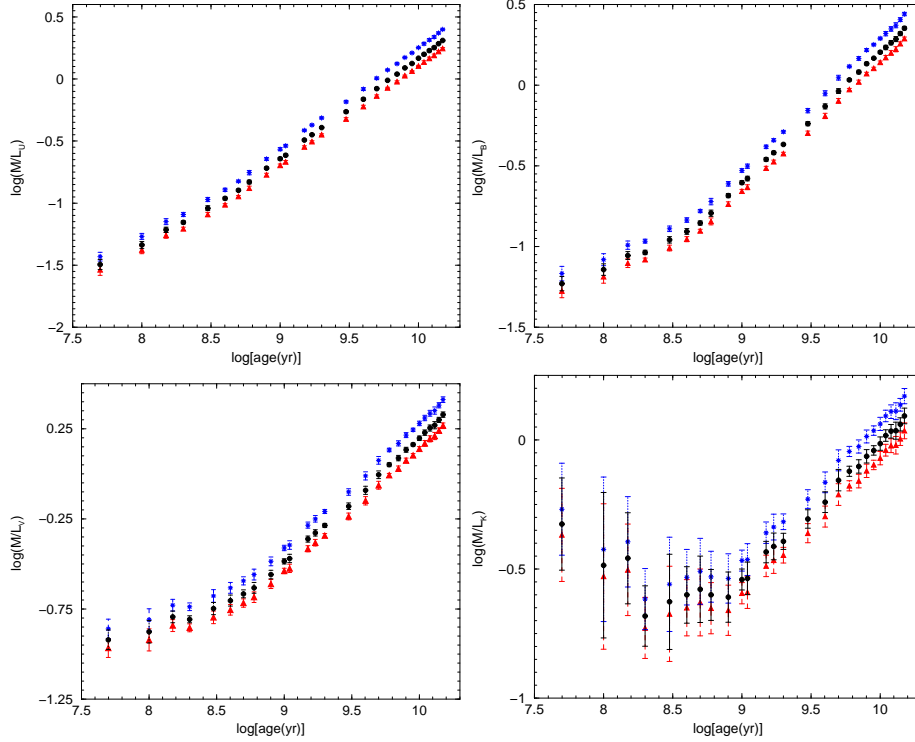


Fig. 11. Time evolution of \mathcal{M}/L (in solar units) in selected passbands (U, B, V, K) for models with $M_V^{tot} = -8$ calculated with the lower, central and upper value for the Kroupa (2002) IMF exponent for $M \leq 0.5M_\odot$. Black dots indicate our reference model ($\alpha = 1.3$), red triangles indicate models with $\alpha = 0.8$ and blue stars models with $\alpha = 1.8$.

spectively. Models with $M_V^{tot} = -8$ mag are plotted in selected passbands while results for other passbands and for $M_V^{tot} = -4$ mag are available at CDS.

The \mathcal{M}/L ratio is more sensitive than integrated colours to the IMF shape, as already noted by Maraston (1998); Bruzual & Charlot (2003); Maraston (2005). From Fig. 11 it is evident that, by decreasing the IMF slope at $M \leq 0.5M_\odot$, the mass of the system decreases, while the luminosity remains almost constant. The final effect is to have smaller \mathcal{M}/L ratios than in the *standard* models ($\alpha = 1.3$). At age lower than few billion years, the uncertainty due to stochastic effects is comparable or larger than the effects of exponent variations. Indeed, the IMF variations can be appreciated at ages of the order of 10^{10} yr. We also find that the uncertainty predicted for $M_V^{tot} = -4$ models prevents to detect significant variations at any age.

A different situation is found in Fig. 12. The mass-to-light ratios slightly depend on IMF for age younger than a few billion years, while they are nearly insensitive at old age. This is because an IMF flatter than $\alpha = 2.3$ at $M \geq 0.5$ (red triangles) requires a total mass smaller than in the *standard* case ($\alpha = 2.3$, black circles) to reach the given luminosity, thus predicting low \mathcal{M}/L_V . The effect is enhanced in young stellar populations in which the total mass is dominated by massive stars. On the other hand, by increasing the exponent up to 2.6 (blue stars), the cluster mass needed to have $M_V = -8$ increases, leading to high

\mathcal{M}/L values. Again, mass-to-light ratios in the NIR bands are more affected by stochastic phenomena.

Finally, note that in the case of small variations ($\alpha = 2 \div 2.6$) explored here, the contribution of massive remnants to the total mass does not significantly change, while it is shown to be effective if large variations ($\alpha = 0.5 \div 3.5$) are adopted, see for a discussion Maraston (1998).

6. Summary and conclusions

In this work we have analyzed the intrinsic uncertainties due to stochastic effects on integrated colours and mass-to-light ratios of metal-poor stellar clusters as a function of the total visual magnitude. The calculations are performed for three different values of M_V^{tot} and for a fine grid of stellar ages. Statistical errors are shown to be crucial, especially in the extreme case $M_V^{tot} = -4$ they are so high as to prevent precise quantitative evaluations for all ages. Calculations are done in the standard UBVRIJHK photometric passbands and in the Hubble Space Telescope bands (WFPC2 and NICMOS systems).

We checked the consistency of our models on observational properties of three metal poor clusters, namely M68, M15, and M30, which differ mainly in the absolute visual magnitude, and HB morphology. For each cluster we were able to reproduce both the features of the observed CMD and the integrated colours, showing that the HB morphology does not influence the photometric indices taken into account.

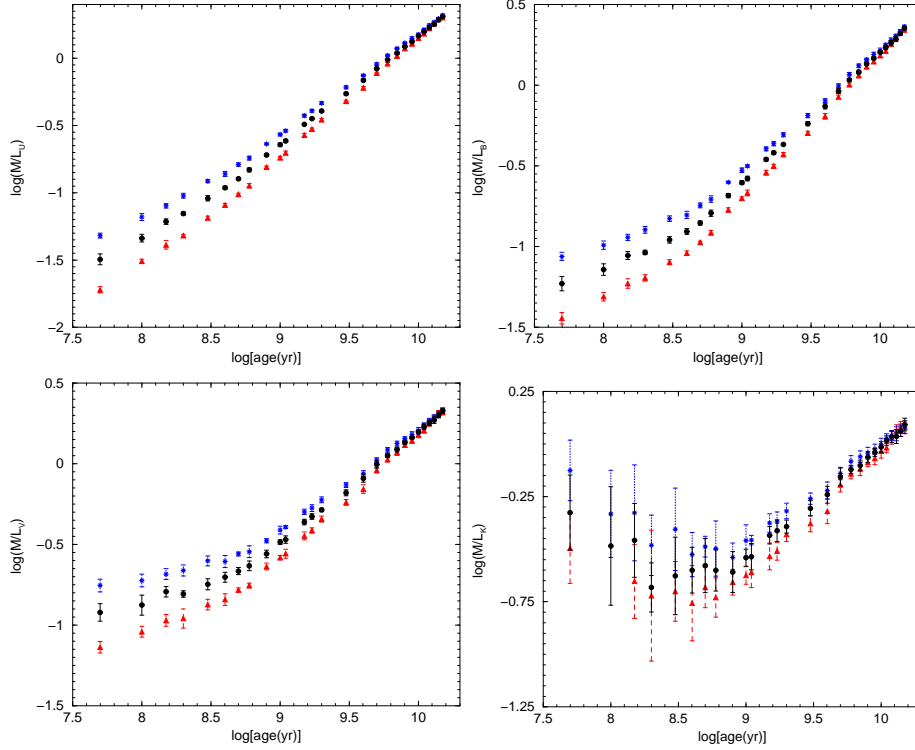


Fig. 12. Time evolution of \mathcal{M}/L (in solar units) in selected passbands (U, B, V, K) for models with $M_V^{tot} = -8$ calculated with the lower, central and upper value for the Kroupa (2002) IMF exponent for $M \geq 0.5M_\odot$. Black dots indicate our reference model ($\alpha = 2.3$), red triangles indicate models with $\alpha = 2.0$, and blue stars indicate models with $\alpha = 2.6$.

A comparisons with recent results available in the literature shows, in some cases, non-negligible differences due to the large variety of prescriptions used in the model calculations.

The uncertainties in the results on both colours and mass-to-light ratios due to the still present uncertainty on the IMF shape have been quantitatively estimated; while the colours fluctuations remains within theoretical uncertainties the \mathcal{M}/L ratio is more sensitive to the IMF shape. We also showed that the influence on \mathcal{M}/L of the adopted value for the minimum mass for which carbon burning is ignite is quite negligible.

Acknowledgements. This work is dedicated to the memory of Vittorio Castellani, whose advise always supported us, and whose enthusiasm and dedication in challenging the astrophysics questions are an invaluable example for all of us. We warmly thank E. Brocato, P.G. Prada Moroni and S.N. Shore for useful discussions and for a careful reading of the manuscript. We are grateful to the anonymous referee for her/his suggestions and comments that greatly improved the paper. Financial support for this work was provided by MIUR-COFIN 2003. This work made use of computational resources granted by the Consorzio di Ricerca del Gran Sasso according to the Progetto 6 ‘*Calcolo Evoluto e sue Applicazioni (RSV6)*’-Cluster C11/B. This paper utilizes the HST-snapshot database by the Globular Cluster Group of the Padova Astronomy Department, and the Catalog of parameters for Milky Way Globular Clusters by W.E. Harris.

References

- Allard F., Hauschildt P.H., Alexander D.R., Starrfield S., 1997, *ARA&A*, 35, 137
- Alves D.R., Bond H.E., Livio M., 2000, *AJ*, 120, 2044
- Anders P., Fritze-v. Alvensleben U., 2003, *A&A*, 401, 1063
- Angeletti L., Dolcetta R., Giannone P., 1980, *Ap&SS*, 69, 45
- Bailyn, C.D., Grindlay, J.E., Cohn, H., Lugger, P.M., Stetson, P.B., Hesser J.E. 1989, *AJ*, 98, 882
- Baraffe I., Chabrier G., Allard F., Hauschildt P.H., 1997, *A&A*, 327, 1054
- Barbaro C., Bertelli C., 1977, *A&A*, 54, 243
- Barmina R., Girardi L., Chiosi C., 2002, *A&A*, 385, 847
- Baud B., Habing H.J., 1983, *A&A*, 127, 73
- Bergeron P., Saumon D., Wesemael F., 1995, *ApJ*, 443, 764
- Bessell M.S., Castelli F., Plez B., 1998, *A&A*, 333, 231
- Blocker T., Herwig F., Driebe T., Bramkamp H., Schonberger D., 1997, In: *IAU Symp. 180: Planetary Nebulae*, 389
- Boily C.M., Lançon A., Deiters S., Heggie D.C., 2005, *ApJ*, 620, L27
- Bombaci I., Parenti I., Vidaña I., 2004, *ApJ*, 614, 314
- Bressan A., Chiosi C., Fagotto F., 1994, *ApJS*, 94, 63
- Brocato E., Caputo F., di Giorgio A.M., Santolamazza P., Richichi A., 1990, *Memorie della Societa Astronomica Italiana*, 61, 137

- Brocato E., Matteucci F., Mazzitelli I., Tornambé A., 1990b, *ApJ*, 349, 458
- Brocato E., Castellani V., Raimondo G., Romaniello M., 1999, *A&AS*, 136, 65
- Brocato E., Castellani V., Poli F.M., Raimondo G., 2000, *A&AS*, 146, 91
- Brocato E., Castellani V., Di Carlo E., Raimondo G., Walker A.R., 2003, *AJ*, 125, 3111
- Bruzual G., Charlot S., 2003, *MNRAS*, 344, 1000
- Burstein D., Faber S. M., Gaskell C. M., Krumm N., 1984, *ApJ*, 287, 586
- Buzzoni A., 1993, *A&A*, 275, 433
- Cardelli J.A., Clayton G.C., Mathis J.S., 1989, *ApJ*, 345, 245
- Cariulo P., Degl'Innocenti S., Castellani V., 2004, *A&A*, 421, 1121
- Carretta E., Gratton R.G., Clementini G., Fusi Pecci F., 2000, *ApJ*, 533, 215
- Castellani V., Chieffi A., Tornambe A., Pulone L., 1985, *ApJ*, 296, 204
- Castellani V., Degl'Innocenti S., Marconi M., Prada Moroni P.G., Sestito P., 2003, *A&A* 404, 645
- Castelli F., 1999, *A&A*, 346, 564
- Castelli F., Gratton R.G., Kurucz R.L., 1997, *A&A*, 318, 841
- Cerviño, M. and Valls-Gabaud, D., 2003, *MNRAS*, 338, 481
- Chabrier G., Baraffe I., 1997, *A&A*, 327, 1039
- Chabrier G., Mera D., 1997, *A&A*, 328, 83
- Charlot S., Bruzual G., 1991, *ApJ*, 367, 126
- Charlot S., Worthey G., Bressan A., 1996, *ApJ*, 457, 625
- Chiosi C., Bertelli G., Bressan A., 1988, *A&A*, 196, 84
- Ciacio F., Degl'Innocenti S., Ricci B., 1997, *A&AS* 123, 449
- Cote P., Marzke R.O., West M.J., 1998, *ApJ*, 501, 554
- De Marchi G., Paresce F. 1994, *ApJ*, 422, 597
- Di Criscienzo M., Marconi M., Caputo F., 2004, *ApJ*, 612, 1092
- Dominguez I., Chieffi A., Limongi M., Straniero O., 1999, *ApJ*, 524, 226
- Fagiolini M., 2004, Diploma Thesis, University of Pisa, Italy
- Fellhauer M., Lin D.N.C., Bolte M., Aarseth S.J., Williams K.A., 2003, *ApJ*, 595, L53
- Ferraro F.R., Messineo M., Fusi Pecci F., et al., 1999, *AJ*, 118, 1738
- Girardi L., Bertelli L., 1998, *MNRAS*, 300, 533
- Girardi L., Bressan A., Bertelli G., Chiosi C., 2000, *A&AS*, 141, 371
- Harris W.E., 1996, *VizieR Online Data Catalog*, 7195, 0
- Harris W.E., 2003, In: *A Decade of Hubble Space Telescope Science*, 78–100
- Hurley J.R., Shara M.M., 2003, *ApJ*, 589, 179
- Kron G.E., Mayall N.U., 1960, *AJ*, 65, 581
- Kroupa P., 2002, *Science*, 295, 82
- Kurth O.M., Fritze-v. Alvensleben U., Fricke K.J., 1999, *A&AS*, 138, 19
- Lattanzio J. C., Wood P. R., 2003, in *Asymptotic giant branch stars*, by Harm J. Habing and Hans Olofsson. Astronomy and astrophysics library, New York, Berlin: Springer, 2003, p. 23 (2003)
- Larsen S.S., 2000, *MNRAS*, 319, 893
- Lee Y., Demarque P., Zinn R., 1994, *ApJ*, 423, 248
- Maeder A., Zahn J., 1998, *A&A*, 334, 1000
- Maraston C., 1998, *MNRAS*, 300, 872
- Maraston C., 2005, *MNRAS*, 362, 799
- Marigo, P., Girardi, L., & Bressan, A. 1999, *A&A*, 344, 123
- Matteucci A., Ripepi V., Brocato E., Castellani V., 2002, *A&A*, 387, 861
- McNamara B.J., Harrison T.E., Baumgardt H., 2004, *ApJ*, 602, 264
- Origlia L., Leitherer C., 2000, *AJ*, 119, 2018
- Palacios A., Talon S., Charbonnel C., Forestini M., 2003, *A&A*, 399, 603
- Pasquali A., De Marchi G., Pulone L., Brigas M. S., 2004, *A&A*, 428, 469
- Pease F.G., 1928, *PASP*, 40, 342
- Piotto G., King I.R., Djorgovski S.G., et al., 2002, *A&A*, 391, 945
- Pols O.R., Schroder K., Hurley J.R., Tout C.A., Eggleton P.P., 1998, *MNRAS*, 298, 525
- Prada Moroni P.G., Straniero O., 2005, *ApJ*, in publication
- Pryor C., Meylan G., 1993, In: *ASP Conf. Ser. 50: Structure and Dynamics of Globular Clusters*, 357
- Raimondo G., Brocato E., Cantiello M., Capaccioli M., 2005, *AJ*, 130, 2625
- Reed B.C., 1985, *PASP*, 97, 120
- Reed B.C., Hesser J.E., Shawl S.J., 1988, *PASP*, 100, 545
- Reimers D., 1975, *Memoires of the Societe Royale des Sciences de Liege*, 8, 369
- Renzini, A., & Buzzoni, A. 1986, in *Proceedings of the Fourth Workshop, Erice, Italy, March 12-22, 1985, Spectral evolution of galaxies* (Dordrecht, D. Reidel Publishing Co.), 195
- Renzini A., Voli M., 1981, *A&A*, 94, 175
- Rey S., Yoon S., Lee Y., Chaboyer B., Sarajedini A., 2001, *AJ*, 122, 3219
- Richard O., Michaud G., Richer J., 2002, *ApJ*, 580, 1100
- Richer J., Michaud G., Rogers F., et al., 1998, *ApJ*, 492, 833
- Rosenberg A., Aparicio A., Saviane I., et al., 2000, *A&AS*, 145, 451
- Salaris M., García-Berro E., Hernanz M., Isern J., Saumon D., 2000, *ApJ*, 544, 1036
- Sandquist E.L., Bolte M., Langer G.E., Hesser J.E., Mendes de Oliveira C., 1999, *ApJ*, 518, 262
- Santos J.F.C., Frogel J.A., 1997, *ApJ*, 479, 764
- Saumon D., Jacobson S.B., 1999, *ApJ*, 511, L107
- Schulz J., Fritze-v. Alvensleben U., Möller C.S., Fricke K.J., 2002, *A&A*, 392, 1
- Spitzer L., 1987, *Dynamical evolution of globular clusters*, Princeton, NJ, Princeton University Press, 1987, 191 p.
- Stetson P.B., 1994, *PASP*, 106, 250
- Straniero O., Dominguez, I., Cristallo, R., Gallino, R. 2003,

- PASA, 20, 389
- Thoul A.A., Bahcall J.N., Loeb A., 1994, ApJ, 421, 828
- Tinsley B.M., 1972, A&A, 20, 383
- Tornambe A., Chieffi A., 1986, MNRAS, 220, 529
- Vazdekis A., 1999, ApJ, 513, 224
- Vesperini E., Heggie D.C., 1997, MNRAS, 289, 898
- Wagenhuber J., Groenewegen M.A.T., 1998, A&A, 340, 183
- Walker A.R., 1994, AJ, 108, 555
- West M.J., Côté P., Marzke R.O., Jordán A., 2004, Nature, 427, 31
- Worthey G., 1994, ApJS, 95, 106
- Yi S.K., 2003, ApJ, 582, 202
- Zhang F., Han Z., Li L., Hurley J.R., 2002, MNRAS, 334, 883
- Zhang F., Li L., Han Z. 2005, MNRAS, 364, 503